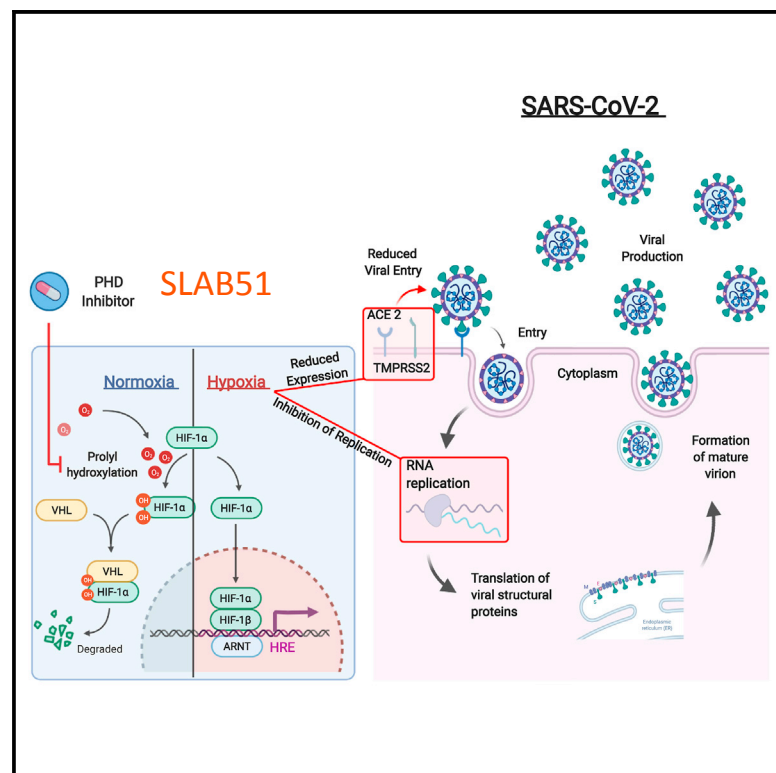


# Hypoxic and pharmacological activation of HIF inhibits SARS-CoV-2 infection of lung epithelial cells

## Graphical abstract



## Authors

Peter A.C. Wing, Thomas P. Keeley, Xiaodong Zhuang, ..., Emma J. Hodson, Tammie Bishop, Jane A. McKeating

## In brief

Wing et al. demonstrate that key aspects of the SARS-CoV-2 life cycle are dependent on cellular oxygen tension. Activation of the cellular oxygen-sensing pathway inhibits SARS-CoV-2 infection, highlighting a key cellular pathway that could be exploited as a potential therapeutic avenue for COVID-19.

## Highlights

- Hypoxia downregulates SARS-CoV-2 receptors ACE2 and TMPRSS2 and inhibits viral entry
- Hypoxic signaling inhibits SARS-CoV-2 replication and particle genesis via HIF-1 $\alpha$
- HIF prolyl hydroxylase inhibitors are a potential therapeutic option for COVID-19 **SLAB 51 is an inhibitor**



## Report

# Hypoxic and pharmacological activation of HIF inhibits SARS-CoV-2 infection of lung epithelial cells

Peter A.C. Wing,<sup>1,2,15</sup> Thomas P. Keeley,<sup>1,3,15</sup> Xiaodong Zhuang,<sup>1</sup> Jeffrey Y. Lee,<sup>4</sup> Maria Prange-Barczynska,<sup>1,3</sup> Senko Tsukuda,<sup>1</sup> Sophie B. Morgan,<sup>5</sup> Adam C. Harding,<sup>6</sup> Isobel L.A. Argles,<sup>1</sup> Samvid Kurlekar,<sup>1</sup> Marko Noerenberg,<sup>4,7</sup> Craig P. Thompson,<sup>8</sup> Kuan-Ying A. Huang,<sup>9,10</sup> Peter Balfe,<sup>1</sup> Koichi Watashi,<sup>11,12</sup> Alfredo Castello,<sup>4,7</sup> Timothy S.C. Hinks,<sup>5</sup> William James,<sup>6</sup> Peter J. Ratcliffe,<sup>1,3,13</sup> Ilan Davis,<sup>4</sup> Emma J. Hodson,<sup>13,14,16</sup> Tammie Bishop,<sup>1,3,16</sup> and Jane A. McKeating<sup>1,2,16,17,\*</sup>

<sup>1</sup>Nuffield Department of Medicine, University of Oxford, Oxford, UK

<sup>2</sup>Chinese Academy of Medical Sciences (CAMS) Oxford Institute (COI), University of Oxford, Oxford, UK

<sup>3</sup>Ludwig Institute for Cancer Research, University of Oxford, Oxford, UK

<sup>4</sup>Department of Biochemistry, University of Oxford, Oxford, UK

<sup>5</sup>Respiratory Medicine Unit and National Institute for Health Research (NIHR) Oxford Biomedical Research Centre (BRC), Nuffield Department of Medicine, Experimental Medicine, University of Oxford, Oxford, UK

<sup>6</sup>Sir William Dunn School of Pathology, University of Oxford, Oxford OX1 3RE, UK

<sup>7</sup>MRC-University of Glasgow Centre for Virus Research, Glasgow, UK

<sup>8</sup>Peter Medawar Building for Pathogen Research, Department of Zoology, University of Oxford, Oxford, UK

<sup>9</sup>Research Center for Emerging Viral Infections, College of Medicine, Chang Gung University, Taoyuan, Taiwan

<sup>10</sup>Division of Pediatric Infectious Diseases, Department of Pediatrics, Chang Gung Memorial Hospital, Taoyuan, Taiwan

<sup>11</sup>Department of Virology II, National Institute of Infectious Diseases, Tokyo 162-8640, Japan

<sup>12</sup>Department of Applied Biological Science, Tokyo University of Science, Noda 278-8510, Japan

<sup>13</sup>Francis Crick Institute, London, UK

<sup>14</sup>Department of Experimental Medicine and Immunotherapeutics, University of Cambridge, Cambridge, UK

<sup>15</sup>These authors contributed equally

<sup>16</sup>Senior author

<sup>17</sup>Lead contact

Correspondence: [jane.mckeating@ndm.ox.ac.uk](mailto:jane.mckeating@ndm.ox.ac.uk)

<https://doi.org/10.1016/j.celrep.2021.109020>

## SUMMARY

COVID-19, caused by the novel coronavirus SARS-CoV-2, is a global health issue with more than 2 million fatalities to date. Viral replication is shaped by the cellular microenvironment, and one important factor to consider is oxygen tension, in which hypoxia inducible factor (HIF) regulates transcriptional responses to hypoxia. SARS-CoV-2 primarily infects cells of the respiratory tract, entering via its spike glycoprotein binding to angiotensin-converting enzyme 2 (ACE2). We demonstrate that hypoxia and the HIF prolyl hydroxylase inhibitor Roxadustat reduce ACE2 expression and inhibit SARS-CoV-2 entry and replication in lung epithelial cells via an HIF-1 $\alpha$ -dependent pathway. Hypoxia and Roxadustat inhibit SARS-CoV-2 RNA replication, showing that post-entry steps in the viral life cycle are oxygen sensitive. This study highlights the importance of HIF signaling in regulating multiple aspects of SARS-CoV-2 infection and raises the potential use of HIF prolyl hydroxylase inhibitors in the prevention or treatment of COVID-19.

The COVID-19 pandemic, caused by the novel coronavirus SARS-CoV-2, is a global health issue. Although multiple public health approaches, including mass vaccination and social distancing, are needed to bring the pandemic under control, there is an urgent need for prophylactic measures or early treatment that can be targeted to vulnerable groups. This is of particular importance given the emergence of SARS-CoV-2 variants and the uncertainty of future vaccine efficacy. SARS-CoV-2 primarily targets the respiratory tract and infection is mediated by spike (S) protein binding to the human angiotensin-converting enzyme 2 (ACE2), where the transmembrane protease serine 2

(TMPRSS2) triggers fusion of the viral and cell membranes (Hoffmann et al., 2020; Wan et al., 2020). ACE2 is highly expressed in epithelial cells of the respiratory tract as well as those of the kidney and intestine (Hamming et al., 2004; Tipnis et al., 2000; Zhao et al., 2020b). Although COVID-19 is mild in most cases, a defining feature of severe disease is systemic low-oxygen levels (hypoxemia), which is often disproportionate to lung injury. There is evidence to suggest that this profound hypoxemia may alter the ability of SARS-CoV-2 to infect host cells. Hypoxia has been reported to regulate the replication of a number of viruses (Jiang et al., 2006; Kraus et al., 2017; Zhao et al., 2020a; Zhuang



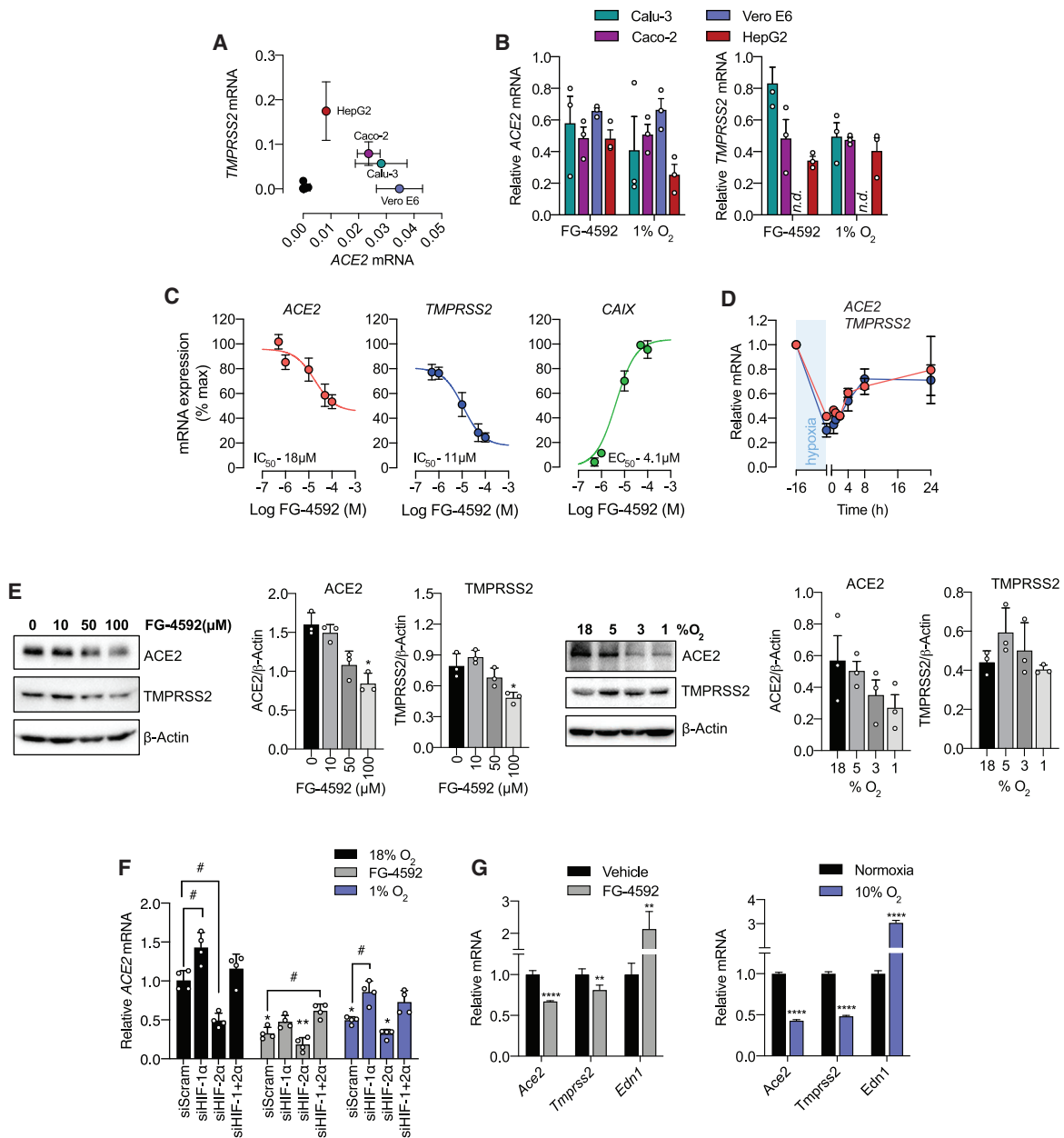


**Figure 1. Hypoxia or FG-4592 (Roxadustat) inhibits the expression of SARS-CoV-2 entry factors *in vitro* and *in vivo***

(A) *ACE2* and *TMPRSS2* transcript levels across a panel of cell lines: HepG2 hepatoma, SH-SY5Y neuronal, RKO colon epithelial, Caco-2 colon epithelial, U937 monocyte/macrophage, Vero E6 monkey epithelial kidney, Calu-3 airway epithelial, A549 airway epithelial, EA.hy926 umbilical vein endothelial, and U-2OS osteosarcoma endothelial. Cells with minimal *ACE2* and *TMPRSS2* mRNA expression (SH-SY5Y, RKO, U937, A549, EA.hy926, and U-2OS) are displayed as black dots. Data are expressed relative to *HPRT* (hypoxanthine-guanine phosphoribosyl transferase).

(B) *ACE2*-expressing cell lines from (A) were treated with FG-4592 (50  $\mu$ M) or 1%  $O_2$  for 24 h, and *ACE2* and *TMPRSS2* mRNA was assessed. Data are presented relative to untreated cells; n.d., not detected.

(C) HepG2 cells were treated with increasing concentrations of FG-4592 for 24 h, and *ACE2/TMPRSS2* mRNA was quantified and expressed as a percentage of the maximal induction/inhibition. *CAIX* mRNA levels were analyzed in parallel as an established HIF-1 $\alpha$ -regulated host gene.

(D) HepG2 cells were cultured at 1%  $O_2$  for 16 h and were re-oxygenated over a 0.5–24-h period, and *ACE2/TMPRSS2* mRNA levels were analyzed at the indicated times.

(E) Calu-3 cells were treated with an increasing concentration of FG-4592 (0–100  $\mu$ M) or 18%, 5%, 3%, and 1%  $O_2$  for 24 h, and *ACE2/TMPRSS2* protein expression was assessed by immunoblot. Densitometric values are expressed relative to  $\beta$ -actin.

(F) siRNAs targeting either HIF-1 or 2 $\alpha$  were delivered into Calu-3 cells individually or in combination. Cells were treated with FG-4592 (50  $\mu$ M) or 1%  $O_2$  for 24 h, and *ACE2* mRNA levels were quantified. Data are expressed relative to the normoxic siScramble (siScram) control. Statistical significance was determined by

(legend continued on next page)

et al., 2020), enhancing the replication of Epstein-Barr virus (Jiang et al., 2006; Kraus et al., 2017), but suppressing HIV and influenza infection (Zhao et al., 2020a; Zhuang et al., 2020), demonstrating that the interaction between hypoxia signaling and viral infection is context specific and dependent on both the host cell and viral species. Furthermore, hypoxia has been reported to either induce or, in some cases, suppress ACE2 expression in lung pulmonary arterial smooth muscle cells (PASMCs) (Zhang et al., 2009, 2019), hematopoietic stem cell precursors (Joshi et al., 2019), and hepatocarcinoma cells (Clarke et al., 2014). Because the effects of low oxygen on both ACE2 expression and SARS-CoV-2 replication are likely to be cell context dependent, we evaluated whether hypoxia alters SARS-CoV-2 entry and replication in lung epithelial cells.

Mammalian cells adapt to low oxygen through an orchestrated transcriptional response regulated by hypoxia-inducible factor (HIF), a heterodimeric transcription factor comprising HIF-1 $\alpha$  or HIF-2 $\alpha$  subunits, which is regulated by oxygen-dependent and -independent stress signals. When oxygen is abundant, newly synthesized HIF $\alpha$  subunits are rapidly hydroxylated by HIF prolyl-hydroxylase domain (PHD) enzymes and are targeted for polyubiquitination and proteasomal degradation. In contrast, when oxygen is limited, HIF $\alpha$  subunits translocate to the nucleus, dimerize with HIF-1 $\beta$ , and activate the transcription of genes involved in cell metabolism, proliferation, pulmonary vasomotor control, and immune regulation (Kaelin and Ratcliffe, 2008; Palazon et al., 2014; Urrutia and Aragonés, 2018). Defining how hypoxia or activation of HIF affects the SARS-CoV-2 life cycle in lung epithelial cells will increase our understanding of disease pathogenesis and inform therapeutic strategies. Specifically, this has the potential for pharmacological intervention because drugs that inhibit the PHD enzymes to stabilize HIF (Pugh and Ratcliffe, 2017; Sanghani and Haase, 2019) are either in advanced clinical trials for the treatment of renal anemia or are licensed for clinical use (Roxadustat in China [Chen et al., 2019a, 2019b] and Japan [Akizawa et al., 2020a, 2020c, 2020d] and Daprodustat in Japan [Akizawa et al., 2020b]).

The host proteins ACE2 and TMPRSS2 are key determinants of SARS-CoV-2 cell entry (Hoffmann et al., 2020). We screened several commonly used cell lines for ACE2 and TMPRSS2 mRNA, and only four demonstrated notable expression of ACE2: HepG2 (hepatoma), Caco-2 (colonic adenocarcinoma), Calu-3 (lung adenocarcinoma), and Vero E6 (monkey kidney epithelia) (Figure 1A). We noted that Vero E6 do not express TMPRSS2 mRNA. To assess the role of HIF in regulating these entry factors, we cultured the cells under hypoxic conditions (1% O<sub>2</sub>) or after being treated with an inhibitor targeting the PHD enzymes (FG-4592/Roxadustat), which stabilizes HIF $\alpha$  subunits and upregulates HIF target gene transcription. Both treatments reduced ACE2 and TMPRSS2 transcripts, with the magnitude of effect varying between cell lines (Figure 1B). Successful

activation of the HIF-signaling pathway was confirmed by induction of the HIF target genes carbonic anhydrase IX (CAIX), N-Myc downstream regulated 1 (NDRG1), and Egl-9 homolog or HIF prolyl hydroxylase 3 (EGLN3 or PHD3) (Figure S1A). In HepG2 cells, in which transcript suppression was most evident, FG-4592 downregulated ACE2 and TMPRSS2 mRNA levels in a dose-dependent manner concomitant with its induction of CAIX, NDRG1, and EGLN3 transcription (Figures 1C and S1B). Reoxygenation of cells previously exposed to hypoxia led to a recovery of both ACE2 and TMPRSS2 mRNA to near pre-hypoxic levels (Figure 1D), suggesting a specific action of the HIF-PHD pathway. To assess whether hypoxia/FG-4592 regulation is evident at the protein level, we also measured ACE2 and TMPRSS2 protein expression in human lung epithelial Calu-3 cells, a more physiologically relevant cell type for studying SARS-CoV-2 infection. Culturing Calu-3 cells under hypoxic conditions or treating with FG-4592 significantly reduced ACE2 protein expression in a dose-dependent manner with maximum suppression >50  $\mu$ M FG-4592 or <3% oxygen (Figure 1E) and no effect on cell viability (Figure S1C). Similar, but more modest, effects were observed with TMPRSS2 expression (Figure 1E). The hypoxia-induced changes in ACE2 (and, to a lesser extent, TMPRSS2) protein expression were observed in HepG2 cells (Figure S1D). Any differences between mRNA and protein levels may, in part, reflect the cleavage and secretion of the TMPRSS2 catalytic domain or that additional hypoxia-stimulated factors regulate protein stability and/or expression. To assess the role of HIF, we silenced HIF-1 $\alpha$  or HIF-2 $\alpha$  expression in hypoxic or FG-4592-treated Calu-3 cells with small interfering RNAs (siRNAs). siRNA-mediated silencing of HIF-1 $\alpha$  (either alone or in combination with HIF-2 $\alpha$ ) restored ACE2 mRNA levels in FG-4592-treated or hypoxic Calu-3 cells (Figure 1F). In contrast, silencing HIF-2 $\alpha$  did not restore ACE2 mRNA levels in either condition tested and resulted in a modest decrease under normoxic conditions (Figure 1F). siRNA knockdown was verified by quantifying the relevant HIF $\alpha$  transcripts CAIX, NDRG1, EGLN3, and VEGFA (Figure S2). These data reveal a role for HIF-1 $\alpha$  in repressing ACE2 mRNA and protein expression.

To expand these observations to an *in vivo* setting, mice were treated with hypoxia (10% O<sub>2</sub>) or FG-4592 for 24 h, with a dosing regimen (oral, 10 mg/kg twice daily) similar to that previously used to induce polycythemia (Schley et al., 2019) and the clinical dose for treating renal anemia (Provenzano et al., 2016). Both treatments reduced *Ace2* and *Tmprss2* transcripts in the lung, along with an increase in Endothelin 1 (*Edn1*) mRNA (Figure 1G), a host gene previously reported to be induced by HIF activation in the respiratory tract (Hickey et al., 2010). Collectively, these data show a role for hypoxia in reducing ACE2 and TMPRSS2 *in vitro* across multiple cell lines, and this is recapitulated in the lungs of mice after systemic hypoxia or FG-4592 treatment.

two-way ANOVA. \*denotes significance relative to normoxic siRNA (siScram) at 18% O<sub>2</sub>, whereas indicates significance relative to the control siRNA per condition.

(G) C57BL/6 mice were treated with FG-4592 (oral, 10 mg/kg twice daily) or 10% O<sub>2</sub> for 24 h, and mRNA expression of *Ace2*, *Tmprss2*, and HIF target gene *Edn1* in the lungs was determined by qPCR.

mRNA expression for each target gene (relative to *Actb*) was compared between biological groups using a Student's two-tailed t test, \*\*p < 0.01, \*\*\*\*p < 0.0001. Data are presented as means  $\pm$  SD from (A–D), n = 3–6; (E) n = 3; (F) n = 4; and (G) n = 4 (n = 3 for *Ace2* in FG-4592 or vehicle-treated mice). See also Figure S1.

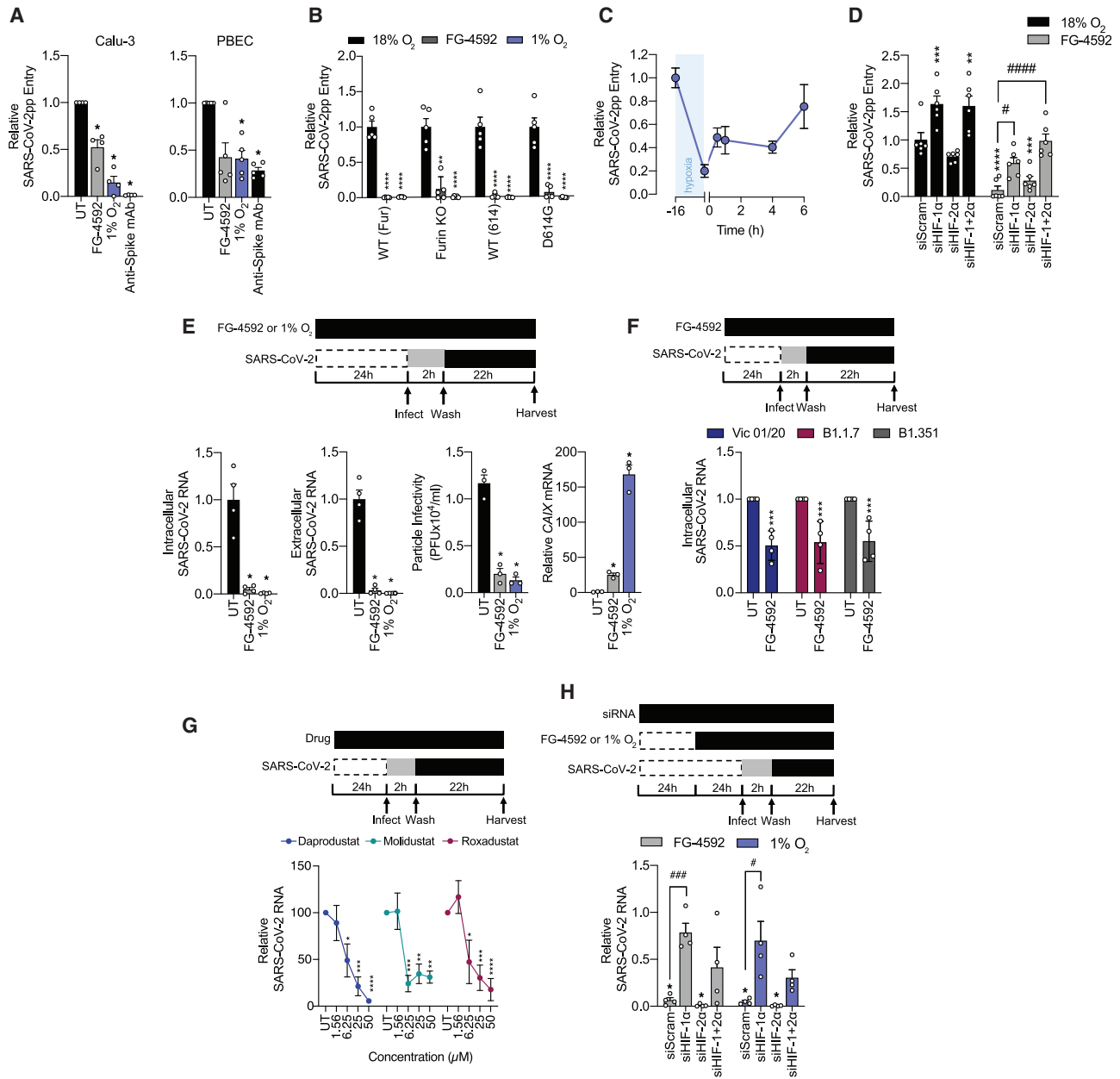


**Figure 2. Hypoxia or FG-4592 (Roxadustat) inhibits SARS-CoV-2 entry in a HIF-1 $\alpha$ -dependent manner**

(A) Calu-3 and primary bronchial epithelial cells (PBECs) pre-treated for 24 h with either FG-4592 (50  $\mu$ M) or 1% O<sub>2</sub> were infected with SARS-CoV-2 pseudo-particle (pp), and infection was measured after 48 h. To demonstrate the specificity of entry via the spike protein, the pp was incubated with anti-spike monoclonal antibody (mAb) FI-3A (1  $\mu$ g/mL) for 30 min before infection. Data are expressed relative to untreated (UT) cells.

(B) Calu-3 cells were treated with FG-4592 (50  $\mu$ M) or 1% O<sub>2</sub> and infected with wild-type (WT) or mutant (D614G or Furin knockout [KO]) SARS-CoV-2pp, and infection was measured 48 h later. Data are expressed relative to UT cells.

(C) Calu-3 cells were cultured at 1% O<sub>2</sub> for 16 h and re-oxygenated over a 0.5–6-h period. Cells were infected with SARS-CoV-2pp at the indicated times, and the pp entry levels were measured 48 h after infection. Data are expressed relative to normoxic cells.

(D) siRNAs against HIF-1 $\alpha$  and HIF-2 $\alpha$  were delivered into Calu-3 cells either individually or in combination. Cells were treated with FG-4592 (50  $\mu$ M) 24 h after transfection and then infected with SARS-CoV-2pp. Data are expressed relative to an siScrambled (siScram) control. \* denotes significance relative to control siRNA (siScram) at 18% O<sub>2</sub>, whereas # indicates significance relative to control siRNA per condition.

(E) Calu-3 cells were treated with FG-4592 (50  $\mu$ M) or cultured at 1% O<sub>2</sub> for 24 h before inoculation with SARS-CoV-2 (MOI 0.001) for 2 h. Infected cells were washed to remove the residual inoculum, and viral replication was assessed 24 h after infection by measuring intracellular and extracellular viral RNA along with infectious titer (particle infectivity) through quantification of plaque-forming units (PFU)/mL. As a control to measure the cellular response to FG-4592 or 1% O<sub>2</sub>, CAIX mRNA was quantified by qPCR. All data (except particle infectivity) is expressed relative to the UT control.

(legend continued on next page)

We hypothesized that the HIF-dependent reduction in ACE2 expression would limit SARS-CoV-2 entry into naive target cells. To assess that, we used lentiviral pseudoparticles (pp) expressing SARS-CoV-2-encoded spike glycoprotein and confirmed that infectivity was ACE2 dependent by infection of human embryonic kidney cells engineered to express ACE2 (Figure S3A). Culturing Calu-3 or primary bronchial epithelial cells (PBECs) under hypoxic conditions or treating with FG-4592 significantly reduced SARS-CoV-2pp infection (Figure 2A). In contrast, viral pp expressing the vesicular stomatitis virus glycoprotein (VSV-G) infected Calu-3 cells and PBEC with comparable efficiency at both oxygen levels (Figure S3B), demonstrating a SARS-CoV-2-specific phenotype. We next sought to test whether hypoxia/FG-4592 limits entry of the novel SARS-CoV-2 spike protein variants; these have emerged throughout the course of the pandemic, with some conferring a fitness advantage to viral entry. The most notable of these to date, D614G, is globally prevalent in the pandemic, consistent with a reported fitness advantage for infecting cells in the upper respiratory tract (Weissman et al., 2021; Korber et al., 2020). Further, deletion of the unique furin cleavage site (which mediates membrane fusion) in the SARS-CoV-2 spike protein has been observed *in vitro* (Davidson et al., 2020) and in animal models of infection (Peacock et al., 2020). Importantly, hypoxia or FG-4592 treatment of Calu-3 cells reduced infection of pp containing either the spike variant to a similar degree as the wild type (Figure 2B). Reoxygenation of hypoxic Calu-3 cells induced a recovery of SARS-CoV-2pp entry (Figure 2C), consistent with our earlier data showing post-hypoxic recovery of ACE2 and TMPRSS2 mRNA levels. Silencing HIF-1 $\alpha$  reversed the anti-viral effect of FG-4592 (Figure 2D), demonstrating that HIF-1 $\alpha$  represses SARS-CoV-2 entry, consistent with its role in regulating ACE2. In contrast, we observed a negligible effect of silencing HIF-2 $\alpha$  on SARS-CoV-2 entry (Figure 2D). In summary, these data show that hypoxic/FG-4592 activation of HIF-1 $\alpha$  represses ACE2 and impairs entry of SARS-CoV-2 entry pp.

We next assessed whether our observations with SARS-CoV-2pp translate to authentic viral replication. Infecting hypoxic (1% O<sub>2</sub>) Calu-3 cells with SARS-CoV-2 (Victoria 01/20 strain) resulted in a 90% reduction in viral RNA compared with that of normoxic cells (Figure 2E). A similar repression in SARS-CoV-2 RNA levels was also observed when culturing Calu-3 cells in 3% oxygen (Figure S4A). Importantly, FG-4592 (50  $\mu$ M) mimicked the hypoxic inhibition of SARS-CoV-2 replication, leading to a significant reduction in the genesis of new particles (Figure 2E). To define whether hypoxia altered the infectivity of SARS-CoV-2 particles,

we assessed the ratio of RNA copies per plaque-forming unit (PFU), finding no significant difference between virus produced from cells at either 18% O<sub>2</sub> or 1% O<sub>2</sub> ( $9.3 \times 10^3 \pm 6.7 \times 10^3$  and  $2.6 \times 10^3 \pm 1.6 \times 10^3$  means  $\pm$  SD. RNA copies/PFU, respectively). Notably, we demonstrated comparable antiviral efficacy of FG-4592 treatment against the recently identified B.1.1.7 (United Kingdom) and B1.351 (South Africa) SARS-CoV-2 variants (Figure 2F). Treating Calu-3 cells with FG-4592 or two additional PHD inhibitors of the same class: Daprodustat and Molidustat, inhibited SARS-CoV-2 replication in a dose-dependent manner with maximal inhibition noted at approximately 6  $\mu$ M (Figure 2G), which is in the range of reported plasma levels in human subjects after oral administration of these drugs at clinical doses (Provenzano et al., 2016). Efficacy of either PHI treatment or hypoxic culture in the activation of HIF was validated by assessing the induction of CAIX mRNA (Figures 2E and S4B). siRNA silencing of HIF-1 $\alpha$ , but not HIF-2 $\alpha$ , in Calu-3 cells reversed the hypoxic or FG-4592-mediated suppression of viral infection, demonstrating a role for HIF-1 $\alpha$  in repressing SARS-CoV-2 RNA replication (Figure 2H). These data show a key role for HIF-1 $\alpha$  in repressing ACE2-dependent, authentic SARS-CoV-2 entry and infection.

To define whether hypoxia signaling regulates additional post-entry steps in the SARS-CoV-2 life cycle, we evaluated the effect of hypoxia on viral replication when applied throughout or after virus inoculation. Hypoxia reduced viral RNA levels in both conditions and at all multiplicities of infection (MOIs) tested (Figure 3A). Importantly, treating SARS-CoV-2-infected Calu-3 with FG-4592 or hypoxia for 24 h significantly reduced both intracellular and extracellular SARS-CoV-2 RNA (Figure 3B). To further define the post-entry effects of HIFs on viral replication, we infected Calu-3 cells and treated them with either FG-4592 or 1% oxygen 8 h later, once replication complexes were established. We noted a significant reduction in intracellular and extracellular viral RNA with both treatments and an induction of CAIX mRNA (Figure 3C), demonstrating a role for HIFs in the regulation of post-entry viral RNA replication.

Given the marked reduction in the cellular viral RNA burden observed under hypoxic conditions, we sought to understand the effect of hypoxia on the initial establishment of viral replication complexes and quantities of positive genomic-strand viral RNA at the single-cell level. Using single-molecule fluorescence *in situ* hybridization (smFISH), we measured the effect of hypoxia and FG-4592 on positive-strand viral RNAs within the first 6 h of infection, which represents the first cycle of infection (eclipse phase) before the secretion of infectious particles (Figure S5).

(F) Calu-3 cells were treated with FG-4592 (50  $\mu$ M) for 24 h before inoculation with SARS-CoV-2 Victoria 01/20, B1.1.7, or B1.351 (MOI 0.003) for 2 h. Infected cells were washed to remove the residual inoculum, and viral replication was assessed 24 h after infection by measuring intracellular viral RNA, and data are expressed relative to the UT control.

(G) Calu-3 cells were treated with increasing concentrations of Daprodustat (GSK: 1278863), Molidustat (Bay 85-3934), and Roxadustat (FG-4592) and were infected with SARS-CoV-2, and viral replication was assessed 24 h later. Data are expressed relative to UT cells.

(H) siRNA targeting either HIF-1 or 2 $\alpha$  was delivered into Calu-3 cells individually or in combination, and 24 h after transfection was treated with FG-4592 (50  $\mu$ M) or 1% O<sub>2</sub> before inoculating with SARS-CoV-2 (MOI 0.001). Intracellular RNA was quantified 24 h after infection, and data are expressed relative to the normoxic siScramble (siScram) control. \* denotes significance relative to the control siRNA (siScram) at 18% O<sub>2</sub>, whereas # indicates significance relative to control siRNA per condition.

Data are presented as means  $\pm$  SD from (A) n = 4 (Calu-3) and n = 5 (PBEC donors); and (B–G) n = 4. Statistical significance was determined using a one-way (A, B, E, and G) or two-way (D and F) ANOVA. \*p or #p < 0.05, \*\*p or ##p < 0.01, \*\*\*p or ###p < 0.001, \*\*\*\*p or ####p < 0.0001. See also Figures S2–S4.

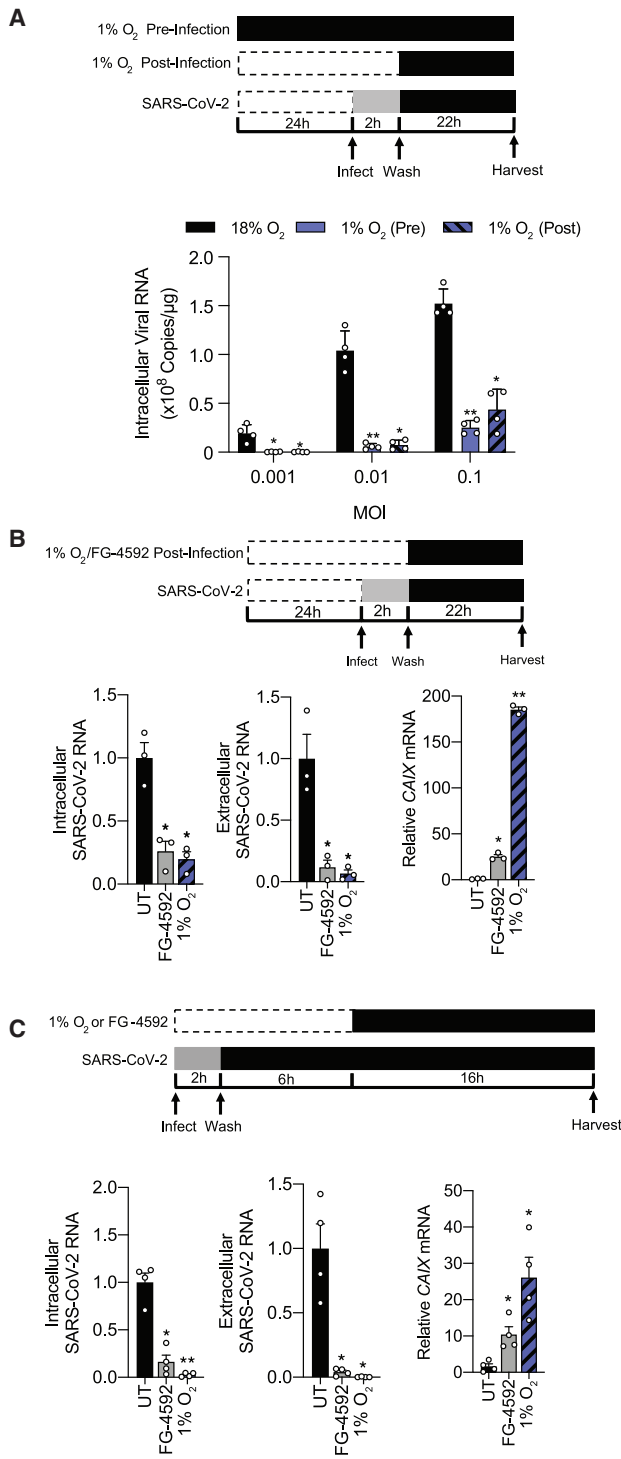


**Figure 3. Hypoxia or FG-4592 (Roxadustat) inhibits SARS-CoV-2 replication post-entry**

(A) Calu-3 cells were treated with 1% O<sub>2</sub> before or after infection with SARS-CoV-2 at the indicated MOIs, and intracellular RNA was quantified by qPCR 24 h later. Data are expressed as RNA copies × 10<sup>8</sup>/μg of total cellular RNA. (B) Calu-3 cells were inoculated with SARS-CoV-2 (MOI 0.001) for 2 h; unbound virus was removed by washing, and cells were treated with FG-4592 (50 μM) or cultured at 1% O<sub>2</sub>. Viral replication was assessed by measuring

Hypoxia and FG-4592 treatment significantly reduced the levels of viral RNA per cell (Figures 4A and 4B). We noted a reduction in the frequency of infected cells, as judged by the detection of genomic RNA (Figure 4C). Because de novo generated viral particles were first detected at 6 h after infection (Figure S5), these RNA signals represent primary infection events.

In conclusion, we describe striking inhibitory effects of hypoxia and FG-4592 (Roxadustat) treatment on SARS-CoV-2 entry (including spike variants), replication, and secretion of infectious particles in lung epithelial cells. These effects were mediated by a HIF-1 $\alpha$ -dependent repression of SARS-CoV-2 replication, in concert with the reduced expression of ACE2 across a range of cell lines and mouse lung tissue. Of note, there are reports of hypoxic induction of ACE2 gene expression in other cell types, albeit often transient (Clarke et al., 2014; Joshi et al., 2019; Zhang et al., 2009). Although this contrasts with our findings, the discrepancy may reflect the minimal ACE2 expression detected in many cell lines we examined, whereas in this study, we focused on cell lines that express greater levels of ACE2 and are relevant to the clinical sites of infection. Alternatively, the reported differences in ACE2 transcriptional regulation may reflect cell-type-specific metabolic phenotypes that modulate HIF signaling (Codo et al., 2020) or expression of co-regulators that mediate indirect effects of HIF stabilization. For example, a study of hypoxic regulation of ACE2 in PASMCS suggests an indirect mechanism through HIF-1 $\alpha$  induction of ACE1 and ANG-II/ATR1 signaling (Zhang et al., 2009); however, ACE1 was not regulated by hypoxia or FG-4592 in Calu-3 cells (Figure S2). Interestingly, recent evidence describes a HIF-1 $\alpha$ -dependent induction of the microRNA LET7b, which directly targets the ACE2 coding sequence to suppress its expression in hypoxic PASMCS (Zhang et al., 2019). Although the precise mechanism by which HIF-1 $\alpha$  represses ACE2 mRNA in lung epithelial cells is unclear, the reversible nature of this repression, combined with the presence of a hypoxia responsive element in the ACE2 promoter (Zhang et al., 2009), may be consistent with direct HIF-mediated repression.

Beyond effects on ACE2-mediated viral entry, we observed marked suppression of SARS-CoV-2 RNA and genesis of infectious particles by hypoxia or pseudohypoxia. Notably, treatment with additional prolyl hydroxylase inhibitors Daprodustat and Molidustat exhibited a comparable antiviral capacity, suggesting a class effect that extends beyond Roxadustat. HIF has been shown to regulate the replication of other RNA viruses through effects on host cell metabolism (Farquhar et al., 2017; Frakolaki et al., 2018; Zhao et al., 2020a). For example, HIF was reported to repress hepatitis C virus replication in the liver via activation of

intra- and extracellular levels of SARS-CoV-2 RNA. The cellular response to FG-4592 or 1% O<sub>2</sub> was assessed through CAIX mRNA quantification. All data are expressed relative to the UT control. Data are presented as means ± SD from (A and B) n = 4, and statistical significance was determined using a two-way ANOVA.

(C) Calu-3 cells were infected with SARS-CoV-2 as detailed above and 8 h later were cultured under 1% O<sub>2</sub> or treated with FG-4592 (50 μM) for 24 h. Intracellular and extracellular viral RNA, along with CAIX transcripts, were measured by qPCR, and data are expressed relative to UT control.

Data are presented as means ± SD from (A–C) n = 4, and statistical significance was determined using a two-way ANOVA. \*p < 0.05, \*\*p < 0.01.

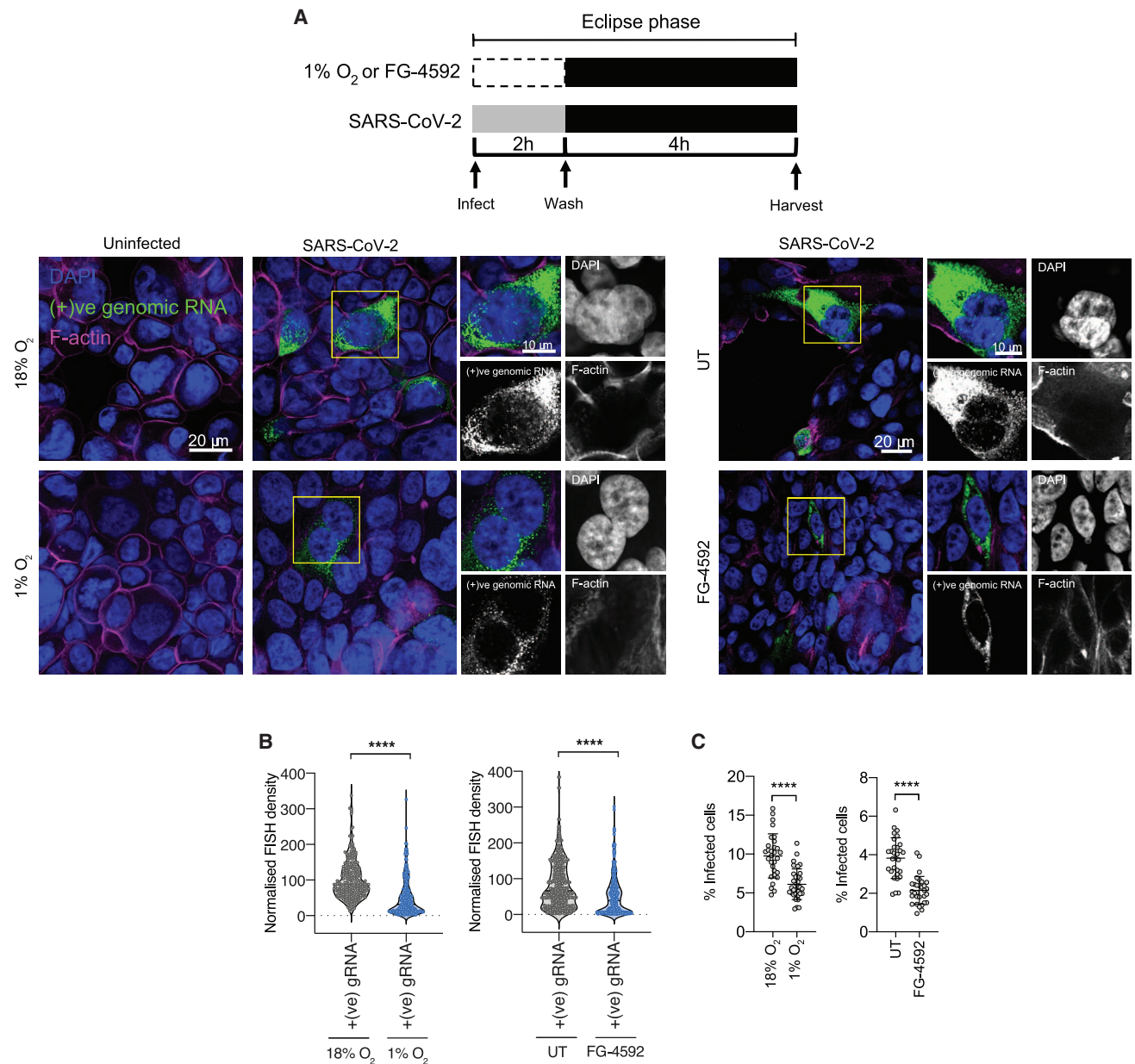


**Figure 4. Hypoxia inhibits SARS-CoV-2 RNA replication**

(A) Calu-3 cells were inoculated with SARS-CoV-2 at an MOI of 1.0 for 2 h; unbound virus was removed by washing, and the cells were cultured at 18% or 1%  $O_2$  or treated with FG-4592 (50  $\mu M$ ) for 4 h. Cells were fixed, and viral infection was visualized by smFISH, where representative two-dimensional (2D) images depicting positive-strand SARS-CoV-2 genomic RNA are shown. Cells are counter-stained with DAPI to visualize the nucleus; inset images show the individual and merged images, and the scale bar depicts 20  $\mu m$ .

(B) Viral RNA was quantified by integrating the three-dimensional (3D) signal density of individual cells, in which each symbol represents a single cell at 18% or 1%  $O_2$  or in FG-4592-treated cells.

(C) The frequency of SARS-CoV-2 positive-strand RNA expressing cells at the different oxygen levels and after FG-4592 treatment was quantified per field of view, in which each symbol reflects a single field.

Data represent the means  $\pm$  SD percentage of viral RNA derived from  $n = 3$ , and significance was assessed by Mann-Whitney test. See also Figure S5.

the autotaxin-lysophosphatidic acid signaling pathway to regulate virus particle genesis (Farquhar et al., 2017). Moreover, our understanding of how HIF regulates respiratory viruses is exemplified by influenza A virus, whose replication was enhanced in mice, with HIF-1 $\alpha$  inactivation restricted to type II alveolar

epithelial cells (Zhao et al., 2020a), highlighting a role for HIF-1 $\alpha$  in repressing this respiratory pathogen. Our findings contrast to those reported by Codo et al. (2020) who showed that treatment of monocytes with the HIF prolyl hydroxylase inhibitor BAY 85-3934 (Molidustat) increased SARS-CoV-2 RNA levels



in an HIF-1 $\alpha$ -dependent manner. This may relate to cell-type-specific differences; for example, monocytes have limited permissivity to support SARS-CoV-2 replication, and viral RNA levels were substantially lower than those measured from infected lung epithelial cells. Further work is needed to characterize the HIF-1 $\alpha$ -dependent mechanisms of SARS-CoV-2 repression described here, which are likely mediated via HIF-1 $\alpha$  regulation of host factors essential for viral RNA replication and/or stability.

Our observations raise clear questions as to how cellular hypoxia translates to humans, both in terms of SARS-CoV-2 susceptibility and clinical progression of COVID-19. There has been some speculation that chronic hypoxia may be protective, with reports of reduced incidence of COVID-19 disease in high-altitude human populations (Pun et al., 2020) (although these observations are complicated by geographic and socioeconomic factors). Some clinical studies suggest that smokers and patients with chronic respiratory diseases (e.g., asthma and COPD) are under-represented co-morbidities in hospitalized patients with COVID-19 (Halpin et al., 2020). However, these conditions are also associated with a higher risk of poor outcomes in established infections (Lippi and Henry, 2020; Sanchez-Ramirez and Mackey, 2020) and, more generally, hypoxemia is a negative prognostic indicator in severe COVID-19 (Berenguer et al., 2020; Petrilli et al., 2020; Yadaw et al., 2020). Although this is seemingly at odds with our findings, clinical hypoxemia is a complex state that reflects multiple pathogenic processes, including vascular inflammation, coagulopathy, and microthrombotic disease (McGonagle et al., 2020; Varga et al., 2020), which may confound any protective effects of hypoxia on SARS-CoV-2 infection.

A key finding from our study is the potential therapeutic application of Roxadustat, and other related HIF prolyl hydroxylase inhibitors, in COVID-19, especially because these act on multiple stages of the viral life cycle (impairing entry and replication) and, as such, may be effective against emerging SARS-CoV-2 variants. These drugs have been developed as erythropoiesis-stimulating agents in patients with anemic and chronic kidney disease and are currently being used in both pre-dialysis and dialysis settings. Thus, it is likely that substantial numbers of patients who are at risk of severe COVID-19 (Williamson et al., 2020; Wu et al., 2020) will be receiving these drugs. Our work highlights the urgent need to monitor these patients for any evidence that PHD inhibitors provide prophylactic and/or therapeutic activity against COVID-19. However, clinical translation of Roxadustat may be complex because HIF has multiple systemic effects that could affect COVID-19 disease progression. Moreover, ACE2 is protective in models of lung injury (Kuba et al., 2005), so it is uncertain whether reducing ACE2 expression would have a net benefit in severe lung disease. Regardless of the potential complexity, the marked effects of Roxadustat in protecting naive cells from SARS-CoV-2 entry and in inhibiting viral replication within infected cells merits further evaluation in animal models and consideration for study in human clinical trials.

## STAR★METHODS

Detailed methods are provided in the online version of this paper and include the following:

- **KEY RESOURCES TABLE**
- **RESOURCE AVAILABILITY**
  - Lead contact
  - Materials availability
  - Data and code availability
- **EXPERIMENTAL MODEL AND SUBJECT DETAILS**
  - Animals
  - Cell culture
  - Viral strains
- **METHOD DETAILS**
  - SARS-CoV-2 pseudoparticle genesis and infection
  - SARS-CoV-2 propagation and infection
  - Immunoblotting
  - RT-qPCR
  - FISH quantification of SARS-CoV-2 RNA
  - Image acquisition and analysis
  - Materials
- **QUANTIFICATION AND STATISTICAL ANALYSIS**

## SUPPLEMENTAL INFORMATION

Supplemental information can be found online at <https://doi.org/10.1016/j.celrep.2021.109020>.

## ACKNOWLEDGMENTS

The authors would like to thank colleagues for the provision of reagents: Anderson Ryan for Calu-3 cells (Oncology Department, University of Oxford); Stephan Urban for HepG2 (University of Heidelberg); Tiong Kit Tan, Lisa Smith, Pramila Rijal, and Alain Townsend for anti-S neutralizing mAb FI-34 (WIMM, Oxford); Ariel Isaacs and Naphak Modhiran for the Spike D614G mutant (University of Queensland); and Daniel Bailey for the Spike Furin knockout KO mutant (Pirbright). Additional thanks to Christopher Pugh, Douglas Dos Santos Passos, Xiaotong Cheng, Becky Norris, Timothy McIver, May Lyster, and Sabina Kyriou for their help in various forms; Darren Blase and Zuzana Bencokova for facilitating virus work in NDMRB; Helene Borrmann for critical reading of the manuscript; Alan Wainman at Micron Oxford (<http://micronoxford.com>) for microscope installation and imaging techniques; and Olympus UK and Europe for their generous loan of an Olympus IXplore SpinSR spinning disk system for the imaging work in this project. The McKeating laboratory is funded by a Wellcome Investigator Award (IA) 200838/Z/16/Z, UK Medical Research Council (MRC) project grant MR/R022011/1, and the Chinese Academy of Medical Sciences (CAMS) Innovation Fund for Medical Science (CIFMS), China (grant number: 2018-I2M-2-002). The Ratcliffe laboratory is funded by the Oxford Branch of the Ludwig Institute for Cancer Research; Wellcome IA 106241/Z/14/Z; the Francis Crick Institute, which receives core funding from Cancer Research UK (FC001501), UK MRC (FC001501), and Wellcome (FC001501); and the Paradiance Foundation. P.J.R., E.J.H., and T.B. are additionally funded by the COVID-19 Research Response Fund, University of Oxford. S.K. is funded by the Clarendon scholarships fund and the Christopher Welch Trust. The Davis laboratory is funded by Wellcome IA 209412/Z/17/Z and Wellcome Strategic Awards 091911/B/10/Z and 107457/Z/15/Z. J.Y.L. is funded by the Medical Sciences Graduate Studentship, University of Oxford. The Hinks laboratory is funded by grants from Wellcome (104553/z/14/z and 211050/Z/18/z) and the National Institute for Health Research (NIHR) Oxford Biomedical Research Centre; the views expressed are those of the authors and not those of the NHS or NIHR.

## AUTHOR CONTRIBUTIONS

P.A.C.W. designed and conducted experiments and co-wrote the manuscript; T.P.K. designed and conducted experiments and co-wrote the manuscript; X.Z. conducted experiments; J.Y.L. conducted experiments; M.P.-B. conducted experiments; S.T. conducted experiments; S.B.M. provided PBECs;

A.C.H. generated virus stocks; I.L.A.A. conducted experiments; S.K. conducted experiments; M.N. conducted experiments; C.P.T. provided reagents; K.-Y.A.H. provided reagents; P.B. conducted statistical analysis; K.W. conducted experiments; A.C. designed imaging experiments; T.S.C.H. provided reagents; W.J. provided advice and reagents; P.J.R. provided advice and co-wrote the manuscript; I.D. designed imaging experiments and co-wrote the manuscript; E.J.H. designed experiments and co-wrote the manuscript; T.B. designed experiments and co-wrote the manuscript; and J.A.M. designed the study and co-wrote the manuscript.

#### DECLARATION OF INTERESTS

E.J.H. is employed under the Cambridge Experimental Medicine Initiative, which is partly funded by AstraZeneca, although they have not been involved in this project. P.J.R. is a scientific cofounder of, and holds equity in, ReOx, a university spin-out company that seeks to develop therapeutic inhibitors of HIF hydroxylases. He is also a non-executive director of Immunocore Holdings. The other authors declare no competing interests.

Received: October 17, 2020

Revised: January 28, 2021

Accepted: March 31, 2021

Published: April 5, 2021

#### REFERENCES

Akizawa, T., Iwasaki, M., Yamaguchi, Y., Majikawa, Y., and Reusch, M. (2020a). Phase 3, randomized, double-blind, active-comparator (darbepoetin alfa) study of oral roxadustat in CKD patients with anemia on hemodialysis in Japan. *J. Am. Soc. Nephrol.* *31*, 1628–1639.

Akizawa, T., Nangaku, M., Yonekawa, T., Okuda, N., Kawamatsu, S., Onoue, T., Endo, Y., Hara, K., and Cobitz, A.R. (2020b). Efficacy and safety of daprodustat compared with darbepoetin alfa in Japanese hemodialysis patients with anemia: a randomized, double-blind, phase 3 trial. *Clin. J. Am. Soc. Nephrol.* *15*, 1155–1165.

Akizawa, T., Otsuka, T., Reusch, M., and Ueno, M. (2020c). Intermittent oral dosing of roxadustat in peritoneal dialysis chronic kidney disease patients with anemia: a randomized, phase 3, multicenter, open-label study. *Ther. Apher. Dial.* *24*, 115–125.

Akizawa, T., Yamaguchi, Y., Otsuka, T., and Reusch, M. (2020d). A Phase 3, multicenter, randomized, two-arm, open-label study of intermittent oral dosing of roxadustat for the treatment of anemia in Japanese erythropoiesis-stimulating agent-naïve chronic kidney disease patients not on dialysis. *Nephron* *144*, 372–382.

Berenguer, J., Ryan, P., Rodríguez-Baño, J., Jarrín, I., Carratalà, J., Pachón, J., Yllescas, M., and Arriba, J.R.; COVID-19@Spain Study Group (2020). Characteristics and predictors of death among 4035 consecutively hospitalized patients with COVID-19 in Spain. *Clin. Microbiol. Infect.* *26*, 1525–1536.

Caly, L., Druce, J., Roberts, J., Bond, K., Tran, T., Kostecki, R., Yoga, Y., Naughton, W., Taiaroa, G., Seemann, T., et al. (2020). Isolation and rapid sharing of the 2019 novel coronavirus (SARS-CoV-2) from the first patient diagnosed with COVID-19 in Australia. *Med. J. Aust.* *272*, 459–462.

Cele, S., Gazy, I., Jackson, L., Hwa, S.-H., Tegally, H., Lustig, G., Giandhari, J., Pillay, S., Wilkinson, E., Naidoo, Y., et al. (2021). Escape of SARS-CoV-2 501Y.V2 variants from neutralization by convalescent plasma. *medRxiv*. <https://doi.org/10.1101/2021.01.26.21250224>.

Chen, N., Hao, C., Liu, B.C., Lin, H., Wang, C., Xing, C., Liang, X., Jiang, G., Liu, Z., Li, X., et al. (2019a). Roxadustat treatment for anemia in patients undergoing long-term dialysis. *N. Engl. J. Med.* *381*, 1011–1022.

Chen, N., Hao, C., Peng, X., Lin, H., Yin, A., Hao, L., Tao, Y., Liang, X., Liu, Z., Xing, C., et al. (2019b). Roxadustat for anemia in patients with kidney disease not receiving dialysis. *N. Engl. J. Med.* *381*, 1001–1010.

Clarke, N.E., Belyaev, N.D., Lambert, D.W., and Turner, A.J. (2014). Epigenetic regulation of angiotensin-converting enzyme 2 (ACE2) by SIRT1 under conditions of cell energy stress. *Clin. Sci. (Lond.)* *126*, 507–516.

Codo, A.C., Davanzo, G.G., Monteiro, L.B., de Souza, G.F., Muraro, S.P., Virgilio-da-Silva, J.V., Prodonoff, J.S., Carregari, V.C., de Biagi Junior, C.A.O., Crunfii, F., et al. (2020). Elevated glucose levels favor SARS-CoV-2 infection and monocyte response through a HIF-1 $\alpha$ /glycolysis-dependent axis. *Cell Metab.* *32*, 498–499.

Davidson, A.D., Williamson, M.K., Lewis, S., Shoemark, D., Carroll, M.W., Heesom, K.J., Zambon, M., Ellis, J., Lewis, P.A., Hiscox, J.A., and Matthews, D.A. (2020). Characterisation of the transcriptome and proteome of SARS-CoV-2 reveals a cell passage induced in-frame deletion of the furin-like cleavage site from the spike glycoprotein. *Genome Med.* *12*, 68.

Farquhar, M.J., Humphreys, I.S., Rudge, S.A., Wilson, G.K., Bhattacharya, B., Ciaccia, M., Hu, K., Zhang, Q., Maily, L., Reynolds, G.M., et al. (2017). Autotaxin-lysophosphatidic acid receptor signalling regulates hepatitis C virus replication. *J. Hepatol.* *66*, 919–929.

Frakolaki, E., Kaimou, P., Moraiti, M., Kalliampakou, K.I., Karampetsou, K., Dotsika, E., Liakos, P., Vassilacopoulou, D., Mavromara, P., Bartenschlager, R., and Vassilaki, N. (2018). The role of tissue oxygen tension in dengue virus replication. *Cells* *7*, 241.

Gaspar, I., Wippich, F., and Ephrussi, A. (2017). Enzymatic production of single-molecule FISH and RNA capture probes. *RNA* *23*, 1582–1591.

Halpin, D.M.G., Faner, R., Sibila, O., Badia, J.R., and Agusti, A. (2020). Do chronic respiratory diseases or their treatment affect the risk of SARS-CoV-2 infection? *Lancet Respir. Med.* *8*, 436–438.

Hamming, I., Timens, W., Bultuis, M.L., Lely, A.T., Navis, G., and van Gooor, H. (2004). Tissue distribution of ACE2 protein, the functional receptor for SARS coronavirus. a first step in understanding SARS pathogenesis. *J. Pathol.* *203*, 631–637.

Huang, K.-Y.A., Tan, T.K., Cehn, T.-H., Huang, C.-G., Harvey, R., Hussain, S., Chen, C.-P., Harding, A., Gilbert-Jaramillo, J., Liu, X., et al. (2020). Plasma-blast-derived antibody response to acute SARS-CoV-2 infection in humans. *BioRxiv*.

Hickey, M.M., Richardson, T., Wang, T., Mosqueira, M., Arguiri, E., Yu, H., Yu, Q.C., Solomides, C.C., Morrissey, E.E., Khurana, T.S., et al. (2010). The von Hippel-Lindau Chuvash mutation promotes pulmonary hypertension and fibrosis in mice. *J. Clin. Invest.* *120*, 827–839.

Hoffmann, M., Kleine-Weber, H., Schroeder, S., Krüger, N., Herrler, T., Erichsen, S., Schiergens, T.S., Herrler, G., Wu, N.H., Nitsche, A., et al. (2020). SARS-CoV-2 cell entry depends on ACE2 and TMPRSS2 and is blocked by a clinically proven protease inhibitor. *Cell* *181*, 271–280.e8.

Jiang, J.H., Wang, N., Li, A., Liao, W.T., Pan, Z.G., Mai, S.J., Li, D.J., Zeng, M.S., Wen, J.M., and Zeng, Y.X. (2006). Hypoxia can contribute to the induction of the Epstein-Barr virus (EBV) lytic cycle. *J. Clin. Virol.* *37*, 98–103.

Joshi, S., Wollenzien, H., Leclerc, E., and Jarajapu, Y.P. (2019). Hypoxic regulation of angiotensin-converting enzyme 2 and Mas receptor in human CD34<sup>+</sup> cells. *J. Cell. Physiol.* *234*, 20420–20431.

Kaelin, W.G., Jr., and Ratcliffe, P.J. (2008). Oxygen sensing by metazoans: the central role of the HIF hydroxylase pathway. *Mol. Cell* *30*, 393–402.

Korber, B., Fischer, W.M., Gnanakaran, S., Yoon, H., Theiler, J., Abfalterer, W., Hengartner, N., Giorgi, E.E., Bhattacharya, T., Foley, B., et al.; Sheffield COVID-19 Genomics Group (2020). Tracking changes in SARS-CoV-2 spike: evidence that D614G increases infectivity of the COVID-19 virus. *Cell* *182*, 812–827.e19.

Kraus, R.J., Yu, X., Cordes, B.A., Sathiamoorthi, S., Iempridee, T., Nawandar, D.M., Ma, S., Romero-Masters, J.C., McChesney, K.G., Lin, Z., et al. (2017). Hypoxia-inducible factor-1 $\alpha$  plays roles in Epstein-Barr virus's natural life cycle and tumorigenesis by inducing lytic infection through direct binding to the immediate-early BZLF1 gene promoter. *PLoS Pathog.* *13*, e1006404.

Kuba, K., Imai, Y., Rao, S., Gao, H., Guo, F., Guan, B., Huan, Y., Yang, P., Zhang, Y., Deng, W., et al. (2005). A crucial role of angiotensin converting enzyme 2 (ACE2) in SARS coronavirus-induced lung injury. *Nat. Med.* *11*, 875–879.

- Lippi, G., and Henry, B.M. (2020). Chronic obstructive pulmonary disease is associated with severe coronavirus disease 2019 (COVID-19). *Respir. Med.* *167*, 105941.
- Livak, K.J., and Schmittgen, T.D. (2001). Analysis of relative gene expression data using real-time quantitative PCR and the  $2^{-\Delta\Delta CT}$  Method. *Methods* *25*, 402–408.
- McGonagle, D., O'Donnell, J.S., Sharif, K., Emery, P., and Bridgewood, C. (2020). Immune mechanisms of pulmonary intravascular coagulopathy in COVID-19 pneumonia. *Lancet Rheumatol.* *2*, e437–e445.
- Palazon, A., Goldrath, A.W., Nizet, V., and Johnson, R.S. (2014). HIF transcription factors, inflammation, and immunity. *Immunity* *41*, 518–528.
- Peacock, T.P., Goldhill, D.H., Zhou, J., Bailion, L., Frise, R., Swann, O.C., Kugathasan, R., Penn, R., Brown, J.C., Sanchez-David, R.Y., et al. (2020). The furin cleavage site of SARS-CoV-2 spike protein is a key determinant for transmission due to enhanced replication in airway cells. *BioRxiv*. <https://doi.org/10.1101/2020.09.30.318311>.
- Petrilli, C.M., Jones, S.A., Yang, J., Rajagopalan, H., O'Donnell, L., Chernyak, Y., Tobin, K.A., Cerfolio, R.J., Francois, F., and Horwitz, L.I. (2020). Factors associated with hospital admission and critical illness among 5279 people with coronavirus disease 2019 in New York City: prospective cohort study. *BMJ* *369*, m1966.
- Provenzano, R., Besarab, A., Sun, C.H., Diamond, S.A., Durham, J.H., Cangiano, J.L., Aiello, J.R., Novak, J.E., Lee, T., Leong, R., et al. (2016). Oral hypoxia-inducible factor prolyl hydroxylase inhibitor roxadustat (FG-4592) for the treatment of anemia in patients with CKD. *Clin. J. Am. Soc. Nephrol.* *11*, 982–991.
- Pugh, C.W., and Ratcliffe, P.J. (2017). New horizons in hypoxia signaling pathways. *Exp. Cell Res.* *356*, 116–121.
- Pun, M., Turner, R., Strapazzon, G., Brugger, H., and Swenson, E.R. (2020). Lower incidence of COVID-19 at high altitude: facts and confounders. *High Alt. Med. Biol.* *21*, 217–222.
- Sanchez-Ramirez, D.C., and Mackey, D. (2020). Underlying respiratory diseases, specifically COPD, and smoking are associated with severe COVID-19 outcomes: a systematic review and meta-analysis. *Respir. Med.* *171*, 106096.
- Sanghani, N.S., and Haase, V.H. (2019). Hypoxia-inducible factor activators in renal anemia: current clinical experience. *Adv. Chronic Kidney Dis.* *26*, 253–266.
- Schley, G., Klanke, B., Kalucka, J., Schatz, V., Daniel, C., Mayer, M., Goppelt-Strube, M., Herrmann, M., Thorsteinsdottir, M., Palsson, R., et al. (2019). Mononuclear phagocytes orchestrate prolyl hydroxylase inhibition-mediated renoprotection in chronic tubulointerstitial nephritis. *Kidney Int.* *96*, 378–396.
- Tegally, H., Wilkinson, E., Giovanetti, M., Iranzadeh, A., Fonseca, V., Giandhari, J., Doolabh, D., Pillay, S., San, E.J., Msomi, N., et al. (2020). Emergence and rapid spread of a new severe acute respiratory syndrome-related coronavirus 2 (SARS-CoV-2) lineage with multiple spike mutations in South Africa. *medRxiv*. <https://doi.org/10.1101/2020.12.21.20248640>.
- Thompson, C.P., Grayson, N., Paton, R., Bolton, J.S., Lourenço, J., Penman, B., Lee, L.N., Odon, V., Mongkolsapaya, J., Chinnakannan, S., et al. (2020). Detection of neutralising antibodies to SARS coronavirus 2 to determine population exposure in Scottish blood donors between March and May 2020. *MedRxiv*.
- Tipnis, S.R., Hooper, N.M., Hyde, R., Karran, E., Christie, G., and Turner, A.J. (2000). A human homolog of angiotensin-converting enzyme. Cloning and functional expression as a captopril-insensitive carboxypeptidase. *J. Biol. Chem.* *275*, 33238–33243.
- Urrutia, A.A., and Aragonés, J. (2018). HIF oxygen sensing pathways in lung biology. *Biomedicines* *6*, 68.
- Varga, Z., Flammer, A.J., Steiger, P., Haberecker, M., Andermatt, R., Zinkernagel, A.S., Mehra, M.R., Schuepbach, R.A., Ruschitzka, F., and Moch, H. (2020). Endothelial cell infection and endotheliitis in COVID-19. *Lancet* *395*, 1417–1418.
- Wan, Y., Shang, J., Graham, R., Baric, R.S., and Li, F. (2020). Receptor recognition by the novel coronavirus from Wuhan: an analysis based on decade-long structural studies of SARS coronavirus. *J. Virol.* *94*, e00127–20.
- Weissman, D., Alameh, M.-G., de Silva, T., Collini, P., Hornsby, H., Brown, R., LaBranche, C.C., Edwards, R.J., Sutherland, L., Santra, S., et al. (2021). D614G spike mutation increases SARS CoV-2 susceptibility to neutralization. *Cell. Host Microbe* *21*, 23–31.e4. <https://pubmed.ncbi.nlm.nih.gov/33306985/>.
- Williamson, E.J., Walker, A.J., Bhaskaran, K., Bacon, S., Bates, C., Morton, C.E., Curtis, H.J., Mehrkar, A., Evans, D., Inglesby, P., et al. (2020). Factors associated with COVID-19-related death using OpenSAFELY. *Nature* *584*, 430–436. [https://www.ncbi.nlm.nih.gov/entrez/query.fcgi?cmd=Retrieve&db=PubMed&list\\_uids=32640463&dopt=Abstract](https://www.ncbi.nlm.nih.gov/entrez/query.fcgi?cmd=Retrieve&db=PubMed&list_uids=32640463&dopt=Abstract).
- Wu, J., Li, J., Zhu, G., Zhang, Y., Bi, Z., Yu, Y., Huang, B., Fu, S., Tan, Y., Sun, J., and Li, X. (2020). Clinical Features of maintenance hemodialysis patients with 2019 novel coronavirus-infected pneumonia in Wuhan, China. *Clin. J. Am. Soc. Nephrol.* *15*, 1139–1145. [https://www.ncbi.nlm.nih.gov/entrez/query.fcgi?cmd=Retrieve&db=PubMed&list\\_uids=32444393&dopt=Abstract](https://www.ncbi.nlm.nih.gov/entrez/query.fcgi?cmd=Retrieve&db=PubMed&list_uids=32444393&dopt=Abstract).
- Yadaw, A.S., Li, Y.C., Bose, S., Iyengar, R., Bunyavanich, S., and Pandey, G. (2020). Clinical predictors of COVID-19 mortality. *medRxiv*.
- Yang, L., Titlow, J., Ennis, D., Smith, C., Mitchell, J., Young, F.L., Waddell, S., Ish-Horowicz, D., and Davis, I. (2017). Single molecule fluorescence in situ hybridisation for quantitating post-transcriptional regulation in *Drosophila* brains. *Methods* *126*, 166–176. [https://www.ncbi.nlm.nih.gov/entrez/query.fcgi?cmd=Retrieve&db=PubMed&list\\_uids=28651965&dopt=Abstract](https://www.ncbi.nlm.nih.gov/entrez/query.fcgi?cmd=Retrieve&db=PubMed&list_uids=28651965&dopt=Abstract).
- Zhang, R., Wu, Y., Zhao, M., Liu, C., Zhou, L., Shen, S., Liao, S., Yang, K., Li, Q., and Wan, H. (2009). Role of HIF-1 $\alpha$  in the regulation ACE and ACE2 expression in hypoxic human pulmonary artery smooth muscle cells. *Am. J. Physiol. Lung Cell. Mol. Physiol.* *297*, L631–L640. [https://www.ncbi.nlm.nih.gov/entrez/query.fcgi?cmd=Retrieve&db=PubMed&list\\_uids=19592460&dopt=Abstract](https://www.ncbi.nlm.nih.gov/entrez/query.fcgi?cmd=Retrieve&db=PubMed&list_uids=19592460&dopt=Abstract).
- Zhang, R., Su, H., Ma, X., Xu, X., Liang, L., Ma, G., and Shi, L. (2019). MiRNA let-7b promotes the development of hypoxic pulmonary hypertension by targeting ACE2. *Am. J. Physiol. Lung Cell. Mol. Physiol.* *316*, L547–L557. [https://www.ncbi.nlm.nih.gov/entrez/query.fcgi?cmd=Retrieve&db=PubMed&list\\_uids=30628484&dopt=Abstract](https://www.ncbi.nlm.nih.gov/entrez/query.fcgi?cmd=Retrieve&db=PubMed&list_uids=30628484&dopt=Abstract).
- Zhao, C., Chen, J., Cheng, L., Xu, K., Yang, Y., and Su, X. (2020a). Deficiency of HIF-1 $\alpha$  enhances influenza A virus replication by promoting autophagy in alveolar type II epithelial cells. *Emerg. Microbes Infect.* *9*, 691–706. [https://www.ncbi.nlm.nih.gov/entrez/query.fcgi?cmd=Retrieve&db=PubMed&list\\_uids=32208814&dopt=Abstract](https://www.ncbi.nlm.nih.gov/entrez/query.fcgi?cmd=Retrieve&db=PubMed&list_uids=32208814&dopt=Abstract).
- Zhao, Y., Zhao, Z., Wang, Y., Zhou, Y., Ma, Y., and Zuo, W. (2020b). Single-cell RNA expression profiling of ACE2, the receptor of SARS-CoV-2. *Am. J. Respir. Crit. Care Med.* *202*, 756–759. <https://pubmed.ncbi.nlm.nih.gov/32663409/>.
- Zhuang, X., Pedroza-Pacheco, I., Nawroth, I., Kliszczak, A.E., Magri, A., Paes, W., Rubio, C.O., Yang, H., Ashcroft, M., Mole, D., et al. (2020). Hypoxic micro-environment shapes HIV-1 replication and latency. *Commun. Biol.* *3*, 376. [https://www.ncbi.nlm.nih.gov/entrez/query.fcgi?cmd=Retrieve&db=PubMed&list\\_uids=32665623&dopt=Abstract](https://www.ncbi.nlm.nih.gov/entrez/query.fcgi?cmd=Retrieve&db=PubMed&list_uids=32665623&dopt=Abstract).

STAR★METHODS

KEY RESOURCES TABLE

REAGENT or RESOURCE	SOURCE	IDENTIFIER
<b>Antibodies</b>		
Rabbit anti-Ace2	Abcam	Cat:Ab108252; RRID:AB_10864415
Mouse anti-TMPRSS2	Santa Cruz Biotechnology	sc-515727
Anti-β-Actin-HRP Conjugate	Abcam	Cat:Ab49900; RRID: AB_867494
Anti-Spike FI-3A	Kind Gift from Prof Alain Townsend	FI-3A
<b>Bacterial and virus strains</b>		
SARS-CoV-2 Victoria 01/20, BVIC01 (Caly et al., 2020)	Public Health England	SARS-CoV-2 Victoria 01/20
SARS-CoV-2 B.1.1.7: 20I/501Y.V1.HMPP1 (Tegally et al., 2020)	Public Health England	SARS-CoV-2 B.1.1.7
SARS-CoV-2 B.1.351: 20I/501.V2.HV001 (Cele et al., 2021)	Centre for the AIDS Programme of Research in South Africa	SARS-CoV-2 B.1.351
<b>Chemicals, peptides, and recombinant proteins</b>		
FG-4592 (Roxadustat)	MedChemExpress	HY-13426
GSK1278863 (Daprodustat)	MedChemExpress	HY-17608
BAY 85-3934 (Molidustat)	MedChemExpress	HY-12654
<b>Critical commercial assays</b>		
CytoTox 96® Non-Radioactive Cytotoxicity Assay	Promega	G1780
<b>Deposited data</b>		
Source data for all figures	Mendeley Data	<a href="https://doi.org/10.17632/yvgx2sgsf6.1">https://doi.org/10.17632/yvgx2sgsf6.1</a>
<b>Experimental models: Cell lines</b>		
RKO	Kind Gift from Professor Ester Hammond	RKO
U2-OS	Kind Gift from Dr. Sebastian Nijman	U2-OS
Caco-2	The Francis Crick Institute Cell Services	Caco-2
Vero-E6	Kind Gift from Professor William James	Vero-E6
SH-SY5Y	Kind Gift from Professor E. Yvonne Jones	SH-SY5Y
Calu-3	Kind Gift from Professor Nicole Zitzmann	Calu-3
U937	The Francis Crick Institute Cell Services	U937
A549	The Francis Crick Institute Cell Services	A549
HepG2	Kind gift from Prof Stephan Urban	HepG2
EA.hy926	Kind Gift from Professor Giovanni Mann	EA.hy926
<b>Experimental models: Organisms/strains</b>		
Mouse: wild-type JAX C57BL/6	Charles River/ in-house breeding at the Functional Genetics Facility of the Wellcome Trust Centre for Human Genetics (University of Oxford)	CR Strain code: 632
<b>Oligonucleotides</b>		
ACE2 forward: GGGATCAGAGATCGGAAGAAGAAA	This Paper	N/A
ACE2 reverse: AGGAGGTCTGAACATCATCAGTG	This Paper	N/A
TMPRSS2 forward: AGGTGAAAGCGGGTGTGAGG	This Paper	N/A
TMPRSS2 reverse: ATAGCTGGTGGTGACCCTGAG	This Paper	N/A

(Continued on next page)

**Continued**

REAGENT or RESOURCE	SOURCE	IDENTIFIER
CAIX forward: CTTGAAGAAATCGCTGAGG	This Paper	N/A
CAIX reverse: TGGAAGTAGCGGCTGAAGTC	This Paper	N/A
EGLN3 forward: CACGAAGTGCAGCCCTCTTA	This Paper	N/A
EGLN3 reverse: TTGGCTTCTGCCCTTCTTCA	This Paper	N/A
NDRG1 forward: TTTGATGTCCAGGAGCAGGA	This Paper	N/A
NDRG1 reverse: ATGCCGATGTCATGGTAGGT	This Paper	N/A
VEGFA forward: TTGCCTTGCTGCTCTACCTCCA	This Paper	N/A
VEGFA reverse: GATGGCAGTAGCTGCGCTGATA	This Paper	N/A
HPRT forward: GACCAGTCAACAGGGGACAT	This Paper	N/A
HPRT reverse: AACACTTCGTGGGGTCCTTTTC	This Paper	N/A
HIF-1a forward: TATGAGCCAGAAGAAGACTTTTAGGC	This Paper	N/A
HIF-1a reverse: CACCTCTTTTGGCAAGCATCCTG	This Paper	N/A
HIF-2a forward: CTGTGTCTGAGAAGAGTAACTTCC	This Paper	N/A
HIF-2a reverse: TTGCCATAGGCTGAGGACTCCT	This Paper	N/A
B2M forward: CTACTGAATTCACCCCCACTG	This Paper	N/A
B2M reverse: ACCTCCATGATGCTGCTTACATG	This Paper	N/A
SARS-CoV-2_N forward: CACATTGGCACCCGCAATC,	This Paper	N/A
SARS-CoV-2_N reverse:GAGGAACGAGAAGAGGCTTG	This Paper	N/A
Ace2 FAM	Thermo Fisher	Mm01159006_m1
Tmprss2 FAM	Thermo Fisher	Mm00443677_m1
Edn1 FAM	Thermo Fisher	Mm00438656_m1
ActB VIC	Thermo Fisher	Mm01205647_g1
siRNA HIF-1A CCAUAUAHAHAUACACAAAtt	Ambion	s6539
siRNA Epas1 (HIF-2A) GUAACUUCUUAUUCACCAAtt	Ambion	s4700
Silencer Select Negative Control siRNA	Ambion	4390843
<b>Recombinant DNA</b>		
pSARS-Spike	Kind gift from Craig Thompson (University of Oxford)	N/A
p8.91 (GAG-POL)	Kind gift from Craig Thompson (University of Oxford)	N/A
pCSFW	Kind gift from Craig Thompson (University of Oxford)	N/A

(Continued on next page)

**Continued**

REAGENT or RESOURCE	SOURCE	IDENTIFIER
pcDNA3.1-hACE2	Kind gift from Craig Thompson (University of Oxford)	N/A
pSpike-D614G	Kind gift from Ariel Isaacs and Naphak Modhiran (University of Queensland)	N/A
pSpike-FurKO	Kind gift from Dalan Bailey (University of Queensland)	N/A
Software and algorithms		
GraphPad 8	Prism	<a href="https://www.graphpad.com">https://www.graphpad.com</a>

**RESOURCE AVAILABILITY**

**Lead contact**

Further information and requests for resources and reagents should be directed to and will be fulfilled by the lead contact, Jane McKeating ([jane.mckeating@ndm.ox.ac.uk](mailto:jane.mckeating@ndm.ox.ac.uk)).

**Materials availability**

This study did not generate new unique reagents.

**Data and code availability**

The authors declare that all data supporting the findings of this study are available in the article. Original data have been deposited to Mendeley Data: <https://doi.org/10.17632/yvgx2sgsf6.1>.

**EXPERIMENTAL MODEL AND SUBJECT DETAILS**

**Animals**

All animal procedures were carried out in accordance with the Animals (Scientific Procedures) Act 1986 Amendment Regulations 2012. Mice were housed in the Functional Genetics Facility of the Wellcome Trust Centre for Human Genetics (University of Oxford) in individually ventilated cages with food and water provided *ad libitum* and on a 13h light/11h dark cycle. Wild-type male mice on a C57BL/6 genetic background, approximately 8 weeks old and littermate controlled were used for the experiments. Mice were treated over the course of 24h with 3 oral gavages of 10mg/kg FG-4592 prepared as a 2.5mg/mL solution in 5mg/mL methyl cellulose, 0.5% Tween80 vehicle (or vehicle alone). Hypoxic mice were housed in a normobaric altitude chamber held at 10% O<sub>2</sub> with controlled temperature, humidity and carbon dioxide levels and compared against mice held in normoxia. Animals were sacrificed by an overdose of Isoflurane (Primal Critical Care) and exsanguination, after which lungs were collected and immediately frozen in liquid nitrogen.

**Cell culture**

RKO, U2-OS, Caco-2 and Vero E6 cell lines were cultured in standard DMEM; SH-SY5Y cell line in DMEM/F-12; Calu-3 in Advanced DMEM; U937 in RPMI; and A549 in F-12K; all supplemented with: 10% fetal bovine serum, 2mM L-glutamine, 100 U/mL penicillin and 10 µg/mL streptomycin. EA.hy926 and HepG2 cells were cultured in standard DMEM additionally supplemented with endothelial cell growth supplement or non-essential amino acids, respectively. All cell lines were maintained at 37°C and 5% CO<sub>2</sub> in a standard culture incubator and exposed to hypoxia using an atmosphere-regulated workstation set to 37°C, 5% CO<sub>2</sub>:1%–5% O<sub>2</sub>:balance N<sub>2</sub> (In-vivo 400, Baker-Ruskinn Technologies). Human PBECs were obtained using flexible fiberoptic bronchoscopy under light sedation with fentanyl and midazolam from healthy control volunteers. Participants provided written informed consent. The study was reviewed by the Oxford Research Ethics Committee B (18/SC/0361). Airway epithelial cells were taken by 2mm diameter cytology brushes from 3rd to 5th order bronchi and cultured in Airway Epithelial Cell medium (PromoCell, Heidelberg, Germany) in submerged culture.

**Viral strains**

SARS-CoV-2 strains: Victoria 01/20 (BVIC01) (Caly et al., 2020) (provided by PHE Porton Down after supply from the Doherty Centre Melbourne, Australia); B1.1.7 (Tegally et al., 2020) (201/501Y.V1.HMPP1) (provided by PHE Porton Down) and B.1.351 (201/501.V2.HV001) (Cele et al., 2021) (Centre for the AIDS Programme of Research in South Africa) were passaged in Vero E6 cells.

## METHOD DETAILS

### SARS-CoV-2 pseudoparticle genesis and infection

SARS-CoV-2 lentiviral pseudoparticles (pp) were generated by transfecting 293T cells with p8.91 (Gag-pol), pCSFW (luciferase reporter) and a codon optimized expression construct pcDNA3.1-SARS-CoV-2-Spike, as previously described (Thompson et al., 2020). The Furin cleavage site mutant was generated by mutagenesis of a pcDNA3.1 based clone expressing a C-terminally flag-tagged SARS-CoV-2 Spike protein (Wuhan-Hu-1 isolate; MN908947.3). The polybasic cleavage site TNSPRRA in SARS-CoV-2 Spike was replaced with the corresponding SARS-CoV variant sequence SLL. The pNBF SARS-CoV2 FL D614G mutant was a kind gift from Dr. Daniel Watterson and Dr. Naphak Modhiran (University of Queensland, Australia) and Furin KO mutant from Dr Daniel Bailey (Pirbright Institute, UK). Supernatants containing viral pp were harvested at 48 and 72h post-transfection. Viral titers were determined by infecting Calu-3 cells with a serial dilution of virus and 48h later measuring cellular luciferase. As a control for non-specific lentivirus uptake, stocks were generated with no envelope glycoprotein (No Env). This control was included in all pp experiments and the luciferase values obtained subtracted from values acquired with the SARS-CoV-2pp. To define spike-dependent infection, SARS-CoV-2pp were incubated with the anti-S-mAb FI-3A (1 $\mu$ g/mL) (Huang et al., 2020) for 30min prior to infection.

### SARS-CoV-2 propagation and infection

Naive Vero E6 cells were infected with SARS-CoV-2 at an MOI of 0.003 and incubated for 48-72h until visible cytopathic effect was observed. At this point, cultures were harvested, clarified by centrifugation to remove residual cell debris and stored at  $-80^{\circ}\text{C}$ . Viral titer was determined by plaque assay. Briefly, Vero E6 cells were inoculated with serial dilutions of SARS-CoV-2 viral stocks for 2h followed by addition of a semi-solid overlay consisting of 1.5% carboxymethyl cellulose (SIGMA). Cells were incubated for 72h, visible plaques enumerated by fixing cells using amido black stain and plaque-forming units (PFU) per mL calculated. For infection of Calu-3 cells with SARS-CoV-2, cells were plated 24h before infection with the stated MOI. Cells were inoculated for 2h after which the residual inoculum was removed with three PBS washes. Unless otherwise stated, infected cells were maintained for 24h before harvesting for downstream applications.

### Immunoblotting

Cell lysates were prepared by washing cells with phosphate buffered saline (PBS), then lysing in Igepal lysis buffer (10mM Tris pH 7.5, 0.25M NaCl, 0.5% Igepal) supplemented with Complete TM protease inhibitor cocktail (Sigma Aldrich) at  $4^{\circ}\text{C}$  for 5min, followed by clarification by centrifugation (3min, 12,000 rpm). Supernatant was mixed with Laemmli sample buffer, separated by SDS-PAGE and proteins transferred to polyvinylidene difluoride membrane (Immobilon-P, Millipore). Membranes were blocked in 5% milk in PBS/0.1% Tween-20, then incubated with anti-ACE2 (Abcam ab108252) or anti-TMPRSS2 (SCBT sc-515727) primary antibodies and appropriate HRP-conjugated secondary antibodies (DAKO). Chemiluminescence substrate (West Dura, 34076, Thermo Fisher Scientific) was used to visualize proteins using a ChemiDoc XRS+ imaging system (BioRad). Anti- $\beta$ -actin-HRP conjugate (Abcam ab49900) and/or Coomassie brilliant blue staining was then used to verify equal protein loading and densitometric analysis performed using ImageJ software (NIH).

### RT-qPCR

Cells were washed in PBS then lysed using Tri-reagent (Sigma), and mRNA extracted by phase separation. Equal amounts of cDNA were then synthesized using the High Capacity cDNA Kit (Applied Biosystems) and mRNA expression determined using Fast SYBR master mix using a StepOne thermocycler (Applied Biosystems) using the  $\Delta\Delta\text{C}_t$  method. See [Key resources table](#) for primer sequences. Frozen lungs were homogenized in RLT buffer (QIAGEN) using a Standard Micro-Homogenizer (ProScientific) and mRNA was extracted using the RNeasy Mini kit (QIAGEN), according to manufacturer's instructions. Equal amounts of cDNA were synthesized using the QuantiTect Reverse Transcription Kit (QIAGEN) and mRNA expression was quantified in triplicates in a duplex quantitative real-time PCR using TaqMan Fast Advanced Master Mix and *Ace2* FAM (Mm01159006\_m1), *Tmprss2* FAM (Mm00443677\_m1), *Edn1* FAM (Mm00438656\_m1) and *Actb* VIC (Mm01205647\_g1) assays (Thermo Fisher). The reaction was carried out in the StepOnePlus Real-Time PCR System (Applied Biosystems).  $\Delta\text{C}_T$  was defined as the difference between the Target gene  $\text{C}_T$  and the *Actb*  $\text{C}_T$ .  $-\Delta\Delta\text{C}_T$  values were calculated for each replicate as follows:  $-(\text{FG-4592 } \Delta\text{C}_T - \text{Vehicle } \Delta\text{C}_T)$  (Livak and Schmittgen, 2001). Fold change in the target gene mRNA expression in each genotype group was expressed as  $2^{-\Delta\Delta\text{C}_T}$ .

### FISH quantification of SARS-CoV-2 RNA

SARS-CoV-2 single-molecule fluorescence *in situ* hybridization (smFISH): smFISH was carried out as previously reported (Yang et al., 2017) with minor modifications. Briefly, cells were grown on #0 round glass coverslips in 24 well plate and fixed in 4% paraformaldehyde for 30min at room temperature. Cells were permeabilised in PBS/0.1% Triton X-100 (PBST) for 10min at room temperature followed by washes in PBS and 2x SSC. Cells were pre-hybridized in prewarmed ( $37^{\circ}\text{C}$ ) wash solution (2x SSC, 10% formamide) twice for 20min each at  $37^{\circ}\text{C}$ . Hybridization was carried out in hybridization solution (2x SSC, 10% formamide, 10% dextran sulfate) containing 500nM FISH probes overnight at  $37^{\circ}\text{C}$ . SARS-CoV-2 positive and negative genomic RNA FISH probes were labeled with ATTO633 and ATTO565 (ATTO-Tec), respectively (See [Table S1](#)), according to published protocols (Gaspar et al., 2017). Individual probe sequences are listed in supplemental data. After the overnight hybridization, cells were washed for

20min in pre-warmed wash solution at 37°C followed by counterstaining with DAPI (1 µg/mL) and Phalloidin-AlexaFluor 488 conjugate (264nM), diluted in wash solution. Cells were then washed once with wash solution for 20min at 37°C and twice with 2xSSC for 5min each at room temperature. Coverslips were dipped in pure water and mounted on slides using Vectashield HardSet (Vector Labs).

### Image acquisition and analysis

Mounted cells were imaged on an Olympus SoRa spinning disc confocal with Orca Flash4 CMOS camera using 60x silicone oil objective (1.3 NA, UPLSAPO60XS2) or 100x silicone oil objective (1.35 NA, UPLSAPO100XS). Specimens were imaged in at least ten different locations per condition and replicate. 3D-stacked images were taken with voxel size of 80nm x 80nm x 200nm in x:y:z and images were deconvolved with maximum likelihood algorithm using cellSens (5 iterations, default PSF, Olympus). Background subtraction was performed on all channels using rolling ball subtraction (radius = 100px) in ImageJ (National Institutes of Health). smFISH signal was quantified using intensity-based methods by manually segmenting individual infected cells using phalloidin stain on a maximum projected image and integrating signal intensity across all slices within region of interest. Integrated intensity was divided by cell volume to obtain signal density per volume, which was normalized by subtracting average signal density of uninfected cells. Infection frequency was quantified per field of view for each 3D image. To get total number of cells, DAPI channel was Gaussian filtered (radius = 10px) in ImageJ and nuclei were automatically counted using spot tool in Imaris (diameter = 6µm, Bitplane). Infected cells were counted manually.

### Materials

All reagents and chemicals were obtained from Sigma-Aldrich (now Merck) unless stated otherwise. Roxadustat, Molidustat and Daprodustat were obtained from either Selleckchem or MedChemExpress. See [Key resources table](#) for details

### QUANTIFICATION AND STATISTICAL ANALYSIS

Data was analyzed using GraphPad Prism version 8.0.2 (GraphPad, San Diego, CA, (USA)). P values < 0.05 were considered significant; significance values are indicated as \*p < 0.05; \*\*p < 0.01; \*\*\*p < 0.001; \*\*\*\*p < 0.0001. Please see individual figure legends for further details.



**Supplemental information**

**Hypoxic and pharmacological activation**

**of HIF inhibits SARS-CoV-2**

**infection of lung epithelial cells**

**Peter A.C. Wing, Thomas P. Keeley, Xiaodong Zhuang, Jeffrey Y. Lee, Maria Prange-Barczynska, Senko Tsukuda, Sophie B. Morgan, Adam C. Harding, Isobel L.A. Argles, Samvid Kurlekar, Marko Noerenberg, Craig P. Thompson, Kuan-Ying A. Huang, Peter Balfe, Koichi Watashi, Alfredo Castello, Timothy S.C. Hinks, William James, Peter J. Ratcliffe, Ilan Davis, Emma J. Hodson, Tammie Bishop, and Jane A. McKeating**

## Supplemental Figures

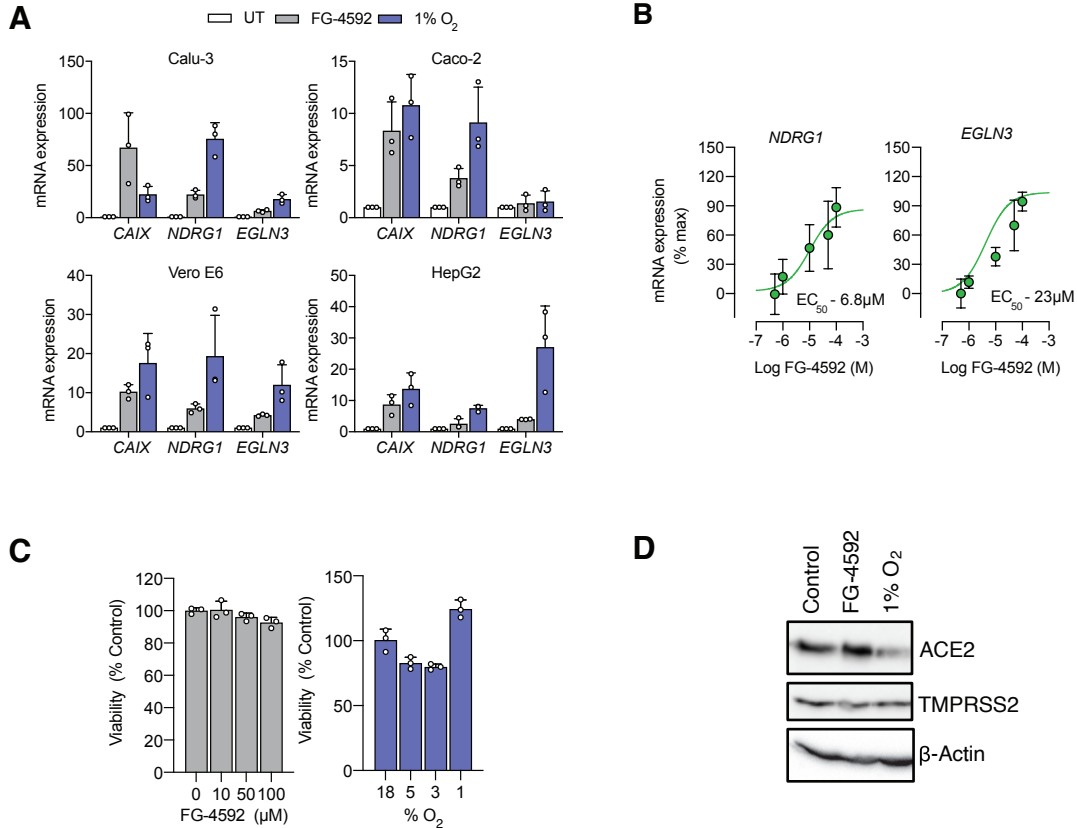


**Fig.S1 Hypoxic gene induction in ACE2 expressing cells. [Related to Fig.1]** (A) Calu-3, Caco-2, Vero E6 and HepG2 cells were treated with FG-4592 (50 $\mu$ M) or 1% O<sub>2</sub> for 24h with *CAIX*, *NDRG1*, and *EGLN3* mRNA assessed by qPCR. Data are expressed relative to normoxic untreated (UT) cells as mean  $\pm$  S.D. from n=3 biological replicates. (B) HepG2 cells were treated with increasing concentrations of FG-4592 for 24h with *NDRG1* and *EGLN3* mRNA quantified. Half-maximal effective concentration (EC<sub>50</sub>) values for both genes in response to FG-4592 treatment were calculated. (C) The impact of either FG-4592 or hypoxic incubation on the viability of Calu-3 cells was assessed through quantification of extracellular lactate dehydrogenase (LDH) 24h post-treatment. (D) HepG2 cells were treated with FG-4592 (50 $\mu$ M) or 1% O<sub>2</sub> for 24h and ACE2/TMPRSS2 protein expression assessed by immunoblot.  $\beta$ -Actin was used to show equal protein loading.

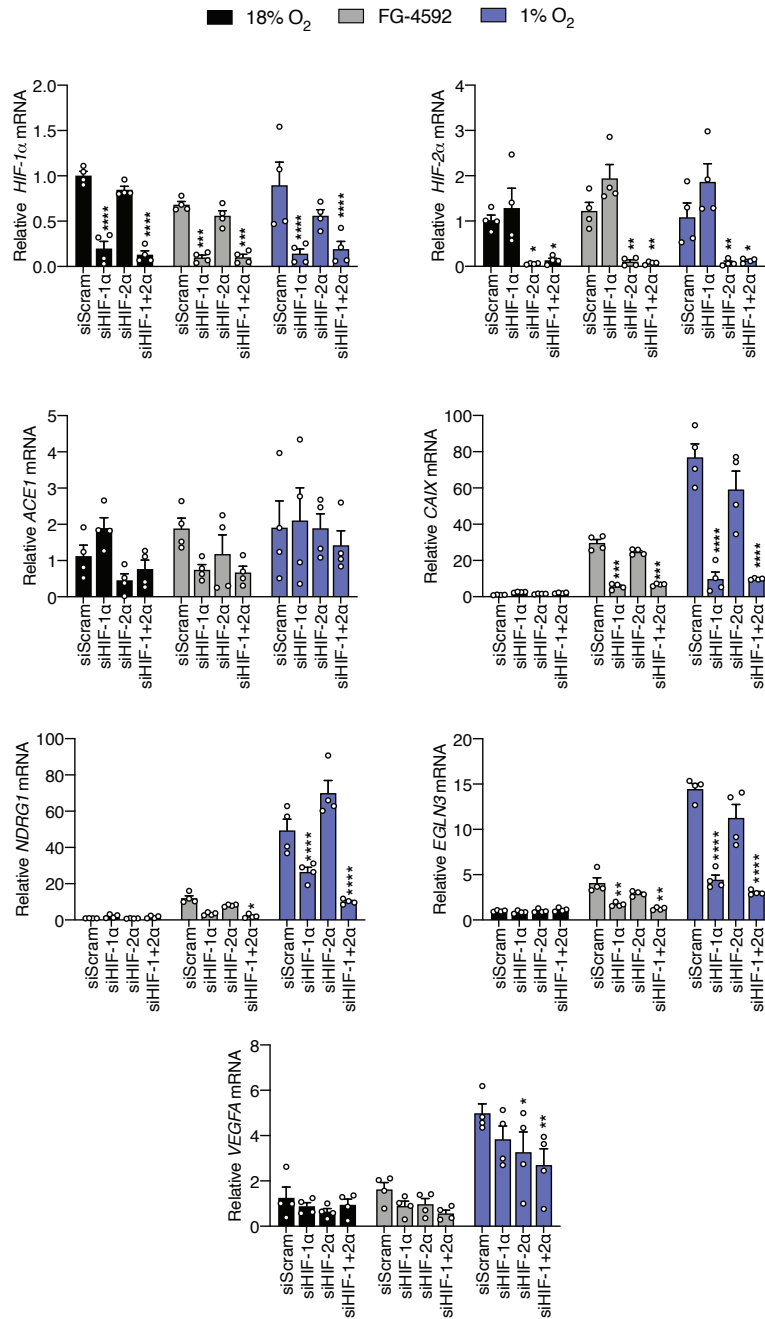


**Fig.S2: Validating siRNA silencing of HIF-1α and HIF-2α in Calu-3 cells. [Related to Fig.2].**

siRNAs targeting either HIF-1 or 2α were delivered into Calu-3 cells either individually or in combination along with a control scrambled siRNA. 48h post-transfection the cells were treated with FG-4592 (50μM) or 1% O<sub>2</sub> for 24h and total cellular RNA extracted. siRNA knock-down was confirmed by qPCR quantification of *HIF-1α*, *HIF-2α*, *ACE1*, *CAIX*, *NDRG1*, *EGLN3* and *VEGFA* mRNA levels. Bars represent mean ± S.D. from n=4 biological replicates and data plotted relative to siScram at 18% O<sub>2</sub> with statistical significance determined by two-way ANOVA, \* p<0.05 \*\* p<0.01, \*\*\* p<0.001, \*\*\*\* p<0.0001.

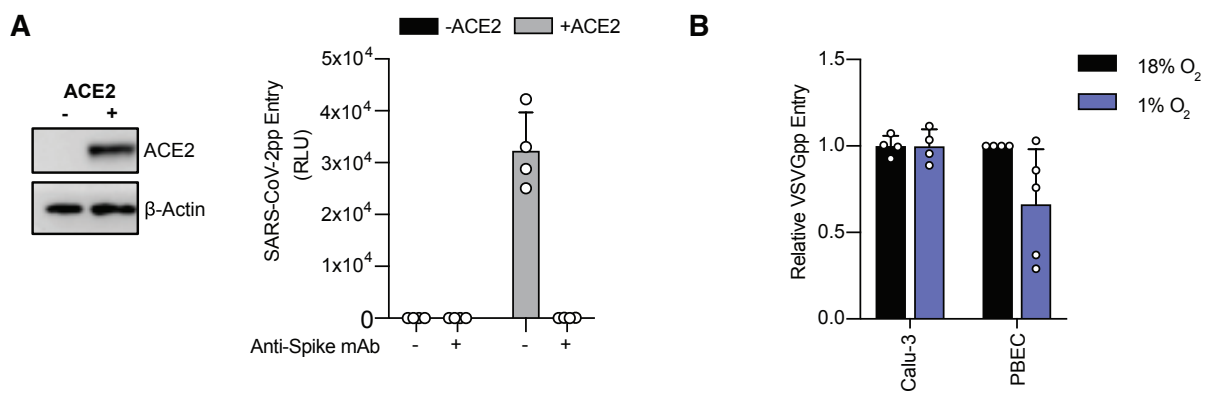


**Fig.S3: SARS-CoV-2pp entry is ACE2 dependent. [Related to Fig.2]. (A)** Human embryonic kidney 293T cells were transfected with a control or human ACE2 overexpression plasmid and infected with SARS-CoV-2 pseudoparticles (pp) 48h post-transfection. ACE2 expression was confirmed by immunoblot. SARS-CoV-2pp were pre-treated with or without an anti-Spike mAb FI-3A (1μg/ml) for 30min prior to infection. Data is mean ± S.D. from n=4 biological replicates. **(B)** Calu-3 or PBECs were cultured under 18% or 1% O<sub>2</sub> for 24h before infection with viral pseudoparticles expressing vesicular stomatitis virus glycoprotein (VSV-G). Infection was assessed 48h later by quantification of luciferase activity. Data is expressed relative to the normoxic samples and is the mean ± S.D. of n=4 biological replicates.

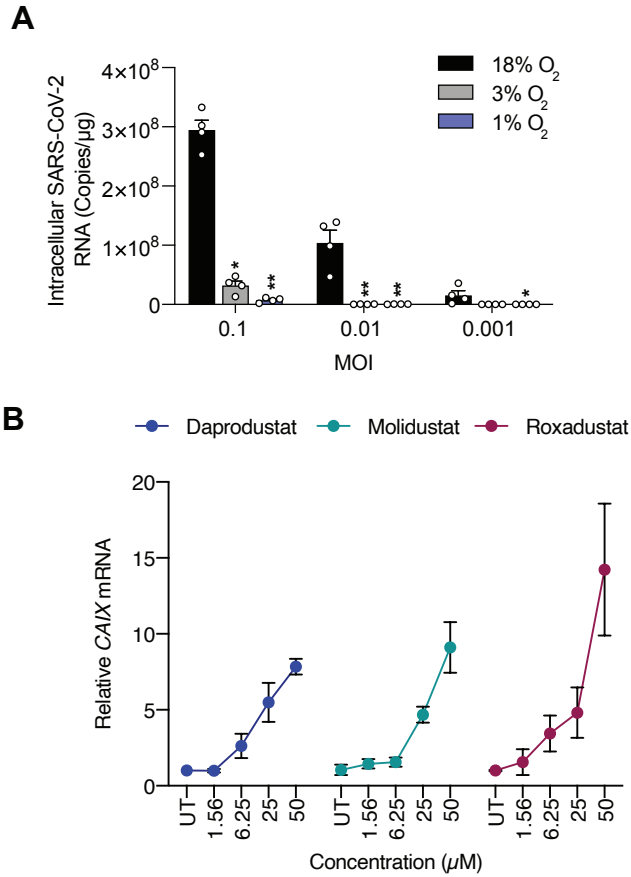


**Fig.S4: Dose dependent Inhibition of SARS-CoV-2 by hypoxia and HIF prolyl hydroxylase inhibitors. [Related to Fig.2].** (A) Calu-3 cells were incubated at 18%, 3% or 1% O<sub>2</sub> for 24h prior to infection with SARS-CoV-2 at the indicated MOIs. Viral RNA was quantified from infected cells 24h post infection. (B) Calu-3 cells were treated increasing concentrations of Daprodustat (GSK1278863), Molidustat (Bay 85-3934) or Roxadustat (FG-4592), infected with SARS-CoV-2 and CAIX mRNA quantified by qPCR. All data is n=4 biological replicates and presented as mean ± S.D. with statistical significance determined by two-way ANOVA, \* p<0.05 \*\* p<0.01.

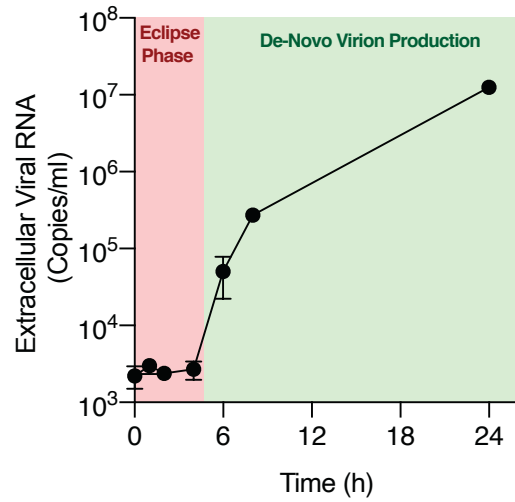


**Fig.S5. Single step growth curve of SARS-CoV-2. [Related to Fig.4].** Calu-3 cells were inoculated with SARS-CoV-2 for 1h at an MOI of 1, unbound virus removed by washing and cells cultured in 18% O<sub>2</sub>. At the indicated times extracellular samples were collected and SARS-CoV-2 RNA quantified by qPCR. Data is presented as mean ± range of n=2 biological replicates.

**Supplementary Table 1: Probe sequences for quantification of SARS-CoV-2 RNA by smFISH [Related to STAR METHODS]**

<b>Positive gRNA probes</b>
TAGATCGGCGCCGTA ACTAT
TCCTTTATTACCGTTCTTAC
AGAAGAACCTTGCCGTAAGC
TACTGAATGCCTTCGAGTTC
AGCATCCGAACGTTTGATGA
TAGTAGTTGTCTGATTGTCC
GTCTTGTTGACCAACAGTTT
CTCATATTGAGTTGATGGCT
AGTAGTATGTAGCCATACTC
TCTAAATCAATGCCAGTGG
GTAATTCAGATACTGGTTGC
CCTTTGAGTGTGAAGGTATT
GAGCAACATAAGCCCGTTAA
AGGTTGTTCTAATGGTTGTA
CATAGGGCTGTTCAAGTTGA
GCTTTTAGAGGCATGAGTAG
TGCGTGACAAATGTTTCACC
AAGGCTTTAAGTTTAGCTCC
CCCAACCGTCTCTAAGAAAC
AAGCCAATCAAGGACGGGTT
TTAGTTAGCCACTGCGAAGT
ACTGAACAACACCACCTGTA
GTAGGCCATTACA ACTAGAT
AGTAGCCAAATCAGATGTGA
TTATAGCGGCCTTCTGTAAA
TTGACGTGCCTCTGATAAGA
TGCGGGAGAAAATTGATCGT
GGCGATCTCTTCATTAAGTT
GGTTGTCATTAAGACCTTCG
ACAACCTATGTTAGCGCTAG
ATAGGCACACTTGTTATGGC
TCCAAAGGCAATAGTGCGAC
AAGACTATGCTCAGGTCCTA
AGTAACCACAAGTAGTGGCA
TCACACTTCATGAGAGTTGA
GCACATTTGGTTGCATTCAT
CAAAGCCACGTACGAGCAGC
GGTGACGCAACTGGATAGAC
CCTTGGTTGAATAGTCTTGA
TTTCAGAACGTTCCGTGTAC
CCAGTTGTTCCGACAAAGTG
TTACCAGCACGTGCTAGAAG
AATGCACTCAAGAGGGTAGC
GTTATCGACATAGCGAGTGT
TAAGCTCACGCATGAGTTCA
CTTCATAAGGATCAGTGCCA
CTCGTCGCCTAAGTCAAATG
GCGAACCTGTAAAACAGGCA